PHOTOGRAPH ENHANCEMENT BY

ADAPTIVE DIGITAL UNSHARP MASKING

by

ALAN MARTIN GILKES

S. B., Massachusetts Institute of Technology
1968

SUBMITTED IN PARTIAL FULFILLMENT

OF THE REQUIREMENTS FOR THE

DEGREE OF MASTER OF

SCIENCE

at the

MASSACHUSETTS INSTITUTE OF TECHNOLOGY
July, 1974

Signature of Author . . . . . .
Department of Electrical Engineering,
July 19, 1974

Certified by . . . . . .
Thesis Supervisor

Accepted by . . . . . .
Chairman, Departmental Committee on Graduate Students

PHOTOGRAPH ENHANCEMENT BY ADAPTIVE DIGITAL UNSHARP MASKING

by

ALAN MARTIN GILKES

Submitted to the Department of Electrical Engineering on July 19, 1974 in partial fulfillment of the requirements for the degree of Master of Science.

ABSTRACT

Image processing systems very often degrade images such that they require appreciable amounts of high-pass filtering or "edge sharpening." This is necessary to enhance the visibility of image details, as well as the aesthetic quality of images. Practical considerations dictate the desirability of sharpening techniques which do not require extensive a priori knowledge of the characteristics of degrading systems. A general knowledge of the brightness and contrast responses of the human visual system led to experimentation with one such sharpening technique: adaptive high-pass filtering. A computer program has been developed which filters a digitized image while varying the frequency response of the filter from one picture element to the next. Unsharp masking is the high-pass filtering technique upon which the program is based. Early experiments with this program used local average brightness as the criterion for selecting the filter frequency response to be used in a particular area of an image. Much greater success was attained in later experiments which used edge contrast as an additional criterion.

All of these adaptive filtering experiments are explained here. In addition, some preliminary experiments with nonadaptive filtering are also recounted. They included both linear and nonlinear high-pass filtering. These experiments demonstrated the strengths and weaknesses of nonadaptive filtering techniques. They also indicated how the enhancing filter's high-frequency response should vary with brightness and contrast, in order to produce the most visually satisfying pictures.

Details of both the design and the performance of the adaptive filtering program are included in this discussion. Possible

modifications to the program for increased speed and efficiency are explained along with suggestions for further research and for other potential applications.

Thesis Supervisor: William F. Schreiber
Title: Professor of Electrical Engineering

ACKNOWLEDGEMENTS

I wish to thank Prof. William F. Schreiber for originally suggesting this work and for his helpful advice and encouragement throughout this research project. I thank Mr. Charles Lynn for invaluable assistance to me in learning the hardware and operating system of the PDP 11/40. Mr. Kenneth Okin was responsible for creating on Dectapes the picture files used in my research. Mr. Robert Piankian devoted great amounts of time and effort to maintaining the CRT Scanner and Laserphoto hardware in the best possible working order, so that my work could proceed at the fastest possible rate. My sincere thanks goes to these two gentlemen as well.

However, the principal acknowledgement for the success of my work must be reserved for my wife, Lolita. The nature and intensity of her encouragement to me and support of me cannot be compared to that of any other person. Her expert typing of these pages is but a small example of that support.

Alan M. Gilkes
July 19, 1974

TABLE OF CONTENTS

TABLE OF FIGURES

IMAGE ENHANCEMENT PROBLEMS AND TECHNIQUES

This thesis details research which investigated the potential usefulness of adaptive image enhancement techniques. The adaptive techniques examined involve nonlinear high-pass filtering of images by a computer program capable of modifying or "adapting" the filter function to certain local characteristics of the image being filtered. Specifically, the computer program treats its input image as a rectangular array of integer brightness values $b(n_1,n_2)$, which is filtered element-by-element into an output image array $B(n_1,n_2)$. The process of "adaptation" involves selecting a "best" filter function to generate each output element $B(n_1,n_2)$, based on relevant characteristics of the input image at or in the neighborhood of (n_1,n_2). Three basic questions arise concerning such a process. First, can an adaptive filtering program operate without excessive use of computer time and storage? The research results presented here will show that it can. Second, can an adaptive filtering program modify filter functions at each picture element (pel) without creating in the output image artifacts which are peculiar to the adaptation process? Research results indicate that the adaptation process not only avoids artifacts of its own but also serves to eliminate some artifacts ordinarily produced by image-independent enhancement techniques. The third question is: Can adaptive filtering demonstrate at least the potential for producing subjectively better output images than image-independent (non-adaptive) filtering techniques? In this

context, "subjectively better" is intended to embrace both a human observer's evaluation of the aesthetic qualities of an output image and his evaluation of how much the visibility of useful information is improved by filtering. Results will show that such a potential definitely exists.

A photograph or electronic image of a given natural scene has, in most cases, a lower spatial bandwidth and dynamic range than the original scene. Although the image is imperfectly derived from the natural scene, it is very often only the first of a series of derivatives. It is the source image from which a family of descendant images is produced by various combinations of processes: electronic scanning, quantization, coding, transmission, and decoding. Frequently, the descendant images are degraded copies of the source image and the three major degradations are:

1. The high frequency content is reduced.
2. There is compression of the brightness differences between objects and their surroundings; the most severe compression usually occurs in bright areas.
3. The noise content is increased.

For these reasons, the filtering operation used to restore descendant images is almost always some form of high-pass filtering or "edge sharpening" which amplifies the high spatial frequencies in the image, while attenuating, if necessary, the very high frequencies in which the noise dominates. Edge sharpening is also useful for enhancing images beyond the requirements of mere restoration of original image quality. A human observer will often judge

a sharpened descendant image to be more informative and more aesthetically satisfying than the source image from which it came.

The literature is rich in explanations of image restoration techniques which involve rigorous application of a priori information about degrading systems to produce an exact or optimal reconstruction of an image. These techniques include inverse filtering [1,2] which requires knowledge of the degrading system's frequency response, and Wiener filtering [3,4] which additionally requires knowledge of signal and noise spectra. In situations where such information is difficult or impossible to gather, it is helpful to appeal to the notion that gathering such information may be unnecessary. The human ability to see and recognize objects in images does not always require exact or least mean square reconstruction of images. There are many image processing systems which do not degrade images so badly that only an exact inversion of the degrading system can reconstruct or improve them. For these reasons, the adaptive filtering research discussed here emphasized the visibility of details in an image, rather than exact or optimal fidelity of the reproduction. Visibility, and the companion idea of relative visibility, were seen as cognitive issues: How easy is it to see and recognize a given bright or dark object, relative to its surroundings in an image? How easy is it to recognize a given object, compared to the ease with which other brighter or darker objects are recognized? Adaptive edge sharpening was investigated as a way of improving a wide variety of images without appeal to detailed a priori knowledge of the degrading systems which produced them. Instead, reference was made to the peculiar spatial frequency and brightness sensitivities

of the human eye. Brightness and contrast were used as criteria to determine how much edge sharpening was required to tailor each image detail to the human observer's needs.

Unsharp masking is a versatile edge sharpening technique well suited to adaptive filtering experiments for two reasons. First, in the frequency domain, one can synthesize any desired high-pass frequency response as the difference between a constant and a low-pass frequency response of appropriate shape. Second, in the spatial domain, it is easy to vary the overshoot/undershoot added to a section of an edge, after a pure "edge signal" devoid of low frequencies has been created. Edge signal generation is done by low-pass filtering (blurring) an image, then subtracting the brightness of the blurred image from the brightness of the original. The process was originally implemented using optical systems and photographic film. Various investigators [5,6] have also implemented electro-optical unsharp masking. These nonadaptive implementations involve subtraction of two video signals by analog circuitry. This thesis discusses a digital implementation of unsharp masking in which the low-pass filtering, the generation of the edge signal, and the weighted addition of the edge signal to the image are all accomplished by computer programs.

Appendix A contains a one-dimensional example of the effect of a linear phase high-pass filter on the edge between a bright and a dark region. This analysis represents linear filtering of brightness (b) as a continuous function of position (x). The analysis shows that the sharpening of the two sides of the edge is symmetric: The peak overshoot

equals the peak undershoot. The peak overshoot does not depend in any way on the average of the brightnesses on either side of the edge. The magnitude of the frequency response at zero frequency is unity. Therefore, a brightness change of a given height is filtered the same way in both bright and dark regions of an image. The peak overshoot does depend on the difference in brightness. Therefore, the brightness peaks at a high-contrast edge may exceed the amplitude limitations imposed by finite dynamic range. The image processing system is then forced to "clip" these peaks to the whitest white and the blackest black.

Homomorphic filtering [7,8,9] makes the action of a linear filter brightness-sensitive. Linear filtering of the logarithm of brightness (density) produces symmetric peaking of the density and asymmetric peaking of the brightness. The asymmetry consists of a peak on the dark side of an edge which has smaller amplitude than the peak on the bright side. Since the brightness sensitivity of humans has been shown [10,11] to be logarithmic, it is reasonable that the amount of edge peaking should increase with increasing brightness. Furthermore, since any additive noise in an image is most visible in dark areas, it is again reasonable that relatively little edge peaking be added in dark areas. Nonlinear characteristics of films and other imaging media would also dictate more edge sharpening in the brightest areas than in the middle tones. Homomorphic filtering has been done [7] with frequency responses whose zero-frequency magnitudes are equal to .5. The action of such a filter, coupled with the effect of logarithmic transformations,

compresses the dynamic range of a filtered image and rebiases the image into the middle of its tone scale. The loss of contrast makes the filtered image appear more uniformly illuminated. A greater degree of edge peaking can be introduced without saturation of blacks or whites. One can argue that such an image is easier for the human eye to examine and easier for imaging systems with finite dynamic range to reproduce.

However, there do exist undesirable features of homomorphic filtering. First of all, the contrast of an image is information, just as are the outlines of objects in the image. Radical reduction of contrast constitutes a reduction in one kind of information available from an image. Secondly, homomorphic filtering creates white halos and black bands along high-contrast edges. (See figures 21(b), 29(a), 30(a), and 30(b) of [7].) It is evident that high-contrast edges need less edge peaking since high contrast is inherently easy to see. Thirdly, the homomorphic filtering of a small change in brightness differs little from linear filtering of that small change. This is because, for small changes in brightness, the logarithmic and exponential functions are piecewise linear, and they are the inverses of one another.

Basic to this investigation of adaptive filtering was the assumption that some nonlinear operator other than the logarithm function can better control the action of a linear filter, according to brightness and contrast criteria. Such an operator should exhibit less of the deficiencies of homomorphic filtering and more of its advantages. In particular, the criteria for measuring the success of the adaptive

filtering experiments were as follows:

1. The filtered image should preserve as much as possible of the dynamic range of the unfiltered image.

2. The various bright and dark objects in the filtered image should receive the maximum edge sharpening possible for each region of the tone scale, subject to three constraints:

(i) High-frequency noise should not be obtrusive in areas of the filtered image containing little high-frequency information.

(ii) High-frequency low-contrast "texture" information, such as grass or wrinkles in clothing should not be sharpened to the point of unnatural appearance.

(iii) The adaptive filtering process should avoid white and black saturation at the high-contrast edges in an image. Compromise between this requirement and the need for preserving dynamic range permits only modest compression of the original image tone scale.

This investigator's original conception of adaptive unsharp masking called for a computer program capable of changing the function used for low-pass filtering from one pel to the next. This requirement placed basic constraints on the filtering algorithm used. It is evident, first of all, that adaptive filtering is at least conceptually simpler if output pels depend not on other output pels but only on the input pels in a certain neighborhood. This argues for "nonrecursive" filter functions; that is, impulse responses of finite extent. An even stronger argument derives from the fact that two-dimensional nonrecursive filters are

never unstable. Recursive filter stability is a much more difficult problem in two dimensions than in one [3]. A second algorithm design decision involved the use of convolution rather than frequency domain filtering. If changing a low-pass filter function from pel to pel involves more than scaling its magnitude, then frequency domain filtering becomes awkward. Sectioning an image into small, possibly irregularly shaped areas for FFT filtering would be costly in both computation and input/output time. In such a circumstance, the possible speed advantages of the FFT over a convolution algorithm would be eliminated. Chapter II will detail the novel convolution algorithm used to accomplish the low-pass filtering. Chapter III will show experimental results indicating that adaptive unsharp masking can operate successfully with a single low-pass filter function. This means that future implementations of the techniques described here can use the speed of the FFT after all. The third basic design decision was that the various filter functions used in adaptive filtering must change very gradually from pel to pel. It was expected that two drastically different filter functions operating in adjoining sections of an image would create visible spurious boundaries. To insure gradual changes from pel to pel in the filtered images, all adaptation algorithms measured the brightness of the low-pass filtered image as the brightness criterion for filter selection.

Before attempting any experiments in adaptive filtering, this investigator did extensive work with the properties of nonadaptive filtering - both linear and nonlinear. This work and the reasons for it, are the subjects of Chapter II.

EXPERIMENTATION WITH NONADAPTIVE FILTERING

A. IMAGE ENHANCEMENT SYSTEM CONFIGURATION

Figure 1 shows the image processing system used for both adaptive and nonadaptive filtering experiments. Photographs of various sizes were mounted on the rotating drum of a Toho Facsimile Transmitter. The photos were scanned at a standard resolution of 100 lines per inch. The analog signal produced for each scan line by the Toho Transmitter was sampled and quantized by a digital interface. The interface output for each scan line was a sequence of eight-bit brightness samples consisting of 100 samples per inch in the direction of scan. These eight-bit pels were recorded on Dectape by the PDP 11/40 computer which was used for all of the image enhancement programs. The computer was programmed to send pictorial output to either or both of two output media. Some digital images were sent in real time through a serial interface to be displayed on the face of a cathode-ray tube flying spot scanner. A Polaroid camera equipped with Polaroid Type 42 film photographed the image on the face of the tube. Other digital images were recorded on disk or tape files. These images were later sent by the computer through a facsimile receiver interface, which reconverted digital sequences to analog scan line signals for a Laserphoto Facsimile Receiver. The Laserphoto recorded the images on dry silver photographic

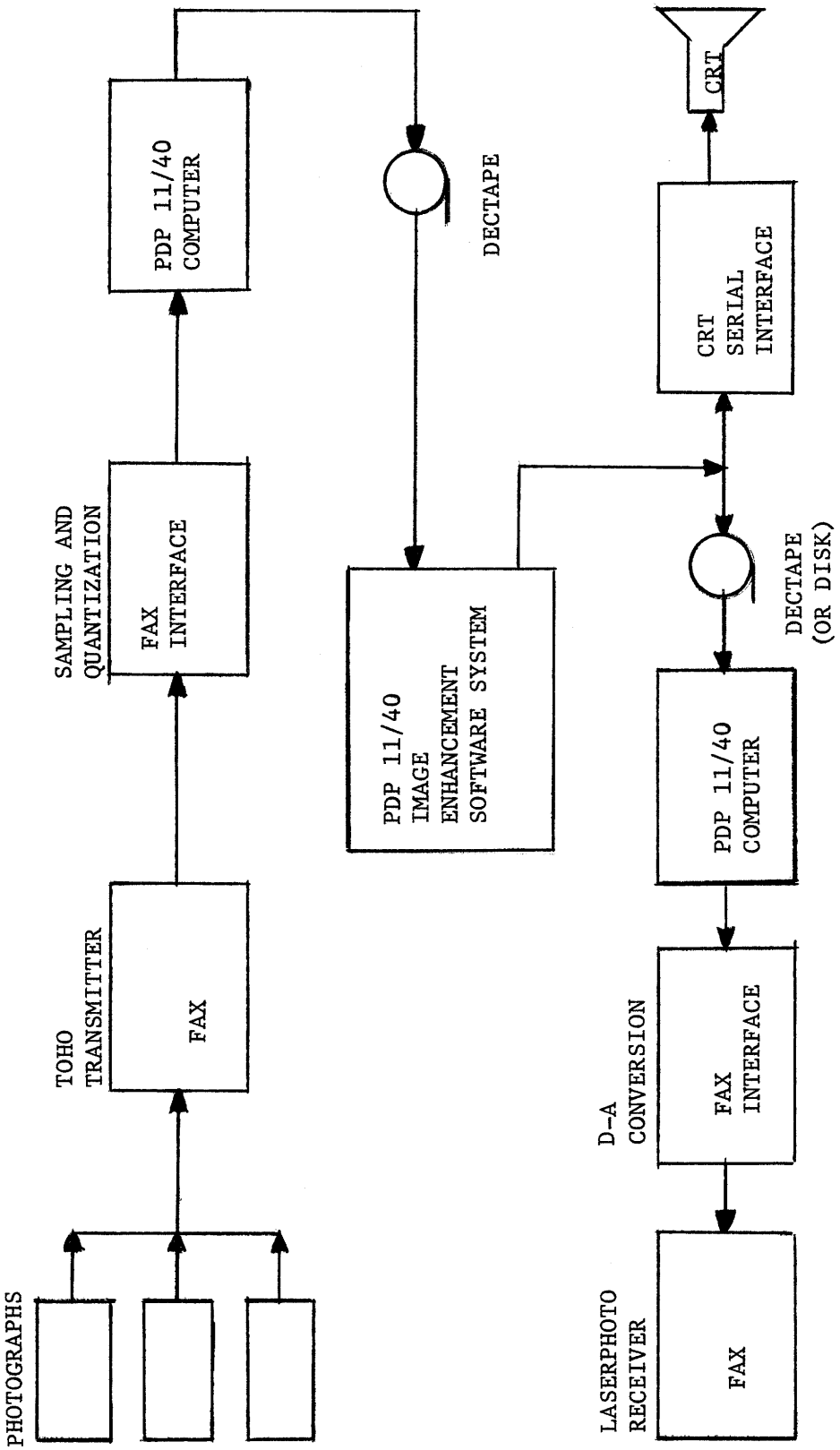

FIGURE 1. TOTAL IMAGE PROCESSING SYSTEM USED FOR THESIS EXPERIMENTS

paper. Viewing this system in light of the discussion in Chapter I, one sees that the original photographs are the source images. The descendant images are those which are recorded without enhancement on Polaroid or dry silver paper. The Toho Transmitter, the facsimile transmitter interface, the facsimile receiver interface, the Laserphoto circuitry, the scanner circuitry and the two different types of film all contribute degradations which determine the appearance of the descendant images. The effect of edge sharpening on these images was judged against the Laserphoto or scanner product, not against the original source photograph. The source photographs merely served as a reference to indicate the amount of detail, the amount of noise, the dynamic range, and the artifacts, if any, in the original image.

The image enhancement computer software identified in Figure 1 consisted of three different subsystems. The subsystem used in the first phase of experiments implemented nonadaptive unsharp masking. This subsystem is shown in Figure 2. The input image $b(n_1,n_2)$ is read in one line at a time from a sequential tape or disk file. Each picture line contains approximately 450 to 670 pels depending on the width of the source photograph. Software switches determine whether or not a logarithmic transformation and a dynamic range compression are performed on the input lines. Since several input lines must be present in memory before the first low-pass filtered output line can be generated, the input lines must be stored in an array. If the point spread function (impulse response or "PSF") of the low-pass

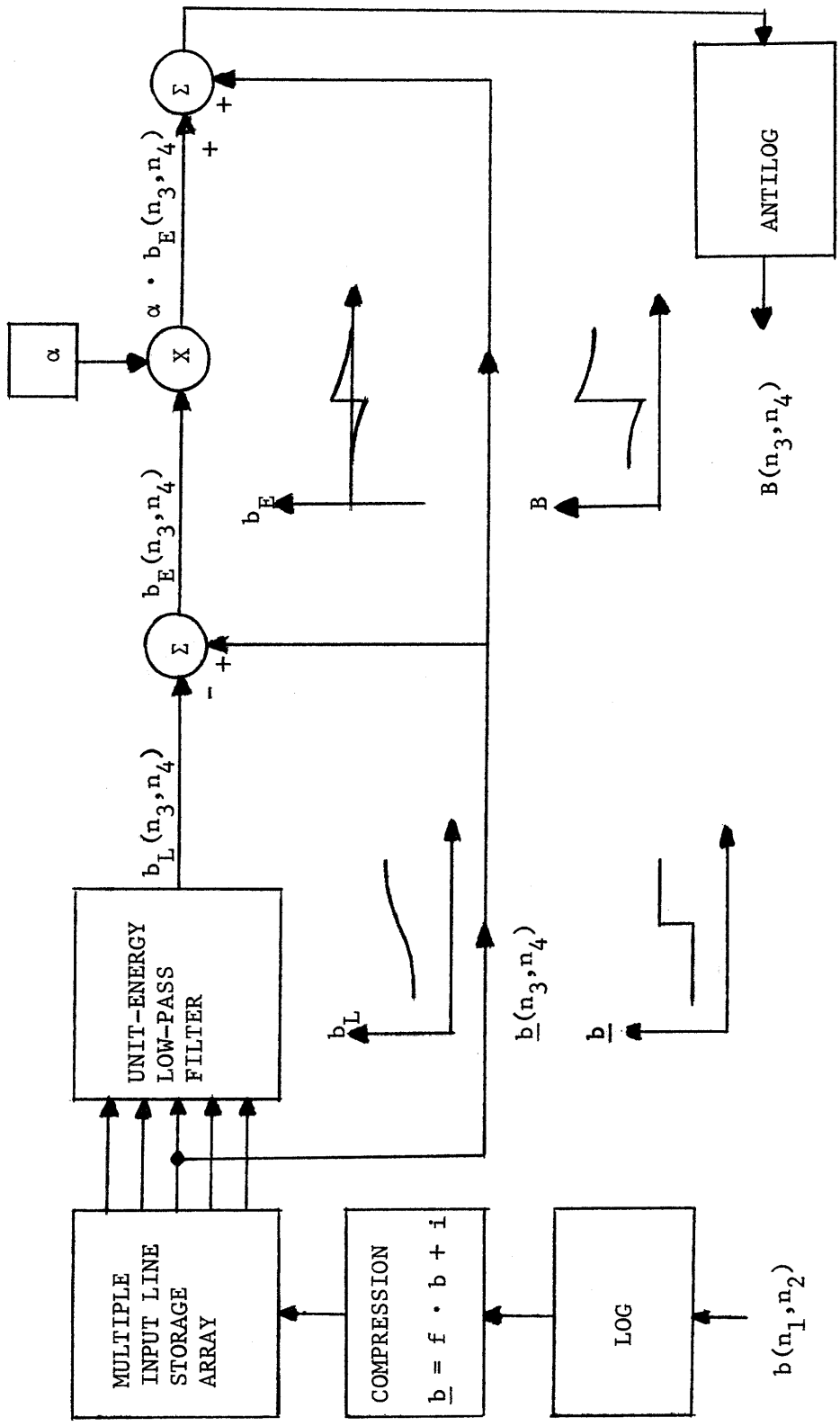

FIGURE 2. IMAGE ENHANCEMENT SOFTWARE SYSTEM FOR NONADAPTIVE FILTERING

filter has a radius of R picture elements, then R picture lines are needed both above and below the input line being filtered. To process the edges of the input image, R border lines containing some constant gray level are supplied at the top and the bottom of the input image. R extra pels are added to the left and right ends of each input picture line. Once a sufficient number of input lines have been stored in the array, the low-pass filter begins generating one output line of the blurred image $b_L(n_3,n_4)$ for each new input line read in. All digital PSF's used in these experiments have unit energy; that is, the magnitude of their frequency response at zero frequency is one. All dynamic range compression is accomplished by the prefiltering compression mentioned above. The software performs the subtraction associated with unsharp masking, after each line of $b_L(n_3,n_4)$ has been generated. The blurred output line is subtracted, pel by pel, from the corresponding line from the input image $\underline{b}(n_3,n_4)$. This input line is one of those available in the multiple line storage array. The result of the subtraction is a line from the edge image $b_E(n_3,n_4)$. For nonadaptive filtering, a single constant "α" multiplies each of the pels of the edge image before the edge image line is added to the input line from $\underline{b}(n_3,n_4)$. This addition sharpens the edges in the input image and the magnitude of α determines the amount of peaking added to each edge. α must, of course, be positive, in order to sharpen, rather than blur, the edges. The sharpening is directly proportional to α. When α is a constant, the filtering and

masking software may be thought of as a linear high-pass filter. The magnitude of its frequency response at zero frequency is one. The high-frequency asymptote of the frequency response is $1 + \alpha$. The precise shape of the frequency response is determined by the frequency response of the low-pass filter. After the sharpened picture line has been generated, the software performs an antilogarithmic transformation on the line, if one is dictated by the setting of a software switch. The final product is a line of the output image $B(n_3,n_4)$ which is then sent by the software to one of the two output media. The following discussion describes the components of this software in greater detail, beginning with the convolutional low-pass filtering algorithm.

B. IMAGE ENHANCEMENT SOFTWARE COMPONENTS: THE LOW-PASS FILTERING ALGORITHM

Useful filtering of images either by optical systems or by digital processors very often involves spatially invariant, linear phase, circularly symmetric PSF's. Among the exceptions to this are filtering operations on images with spatially variant degradations [12] or motion degradations [13,14,15]. When a continuous, circularly symmetric PSF is sampled on a Cartesian grid, and the sample density is high enough to prevent frequency aliasing, the resulting sequence retains approximate circular symmetry. The Fourier transform of such a sequence also demonstrates circular symmetry in a region surrounding (ω_1=0, ω_2=0) in the frequency plane, even though the transform is periodic in ω_1 and ω_2. One may therefore think of using a circularly symmetric discrete sequence $h(n_1,n_2)$ as the digital PSF in a filtering program.

As explained above, early design considerations of adaptive filtering software seemed to make a direct convolution algorithm very desirable. Circular symmetry was seen as a property which could be exploited to economize on the time and storage requirements of a convolution algorithm. During the course of this research, this investigator found no evidence in current literature of any effort toward the study of convolution algorithms based on circular symmetry.

Only one publication [16] even suggests the germ of the idea upon which such algorithms could be based. An original algorithm for circular convolution of functions in Cartesian space is presented here.

The convolution sum equation describes the basic process of filtering an image directly in the spatial domain:

$$B(n_1,n_2) = \sum_{k=-\infty}^{\infty} \sum_{r=-\infty}^{\infty} h(k,r) \cdot b(n_1-k,\ n_2-r)$$

where h, b, and B are the two-dimensional sequences for the PSF, the input image, and the output image, respectively. If finite limits are placed on the indices k and r, then the equation describes convolution of an input image with a PSF of finite extent. If h(k,r) is circularly symmetric about the point (0,0), then it is a linear phase filter.

Further examination of the convolution sum shows how the associated computations can be abbreviated. Since h(k,r) is circularly symmetric, h(k,r) has the same value at every point (k,r) such that:

$$k^2 + r^2 = R^2$$

These points are (k,r), (-k,r), (r,k), (-r,k), (-k,-r), (k, -r), (-r,-k) and (r,-k). Obviously, this eight-fold symmetry reduces to only a four-fold symmetry if k=r or if either k or r is zero. However, one can still reduce the number of multiplications required by

the convolution sum. All of the b values on a ring of radius R may be added before the sum is multiplied by h(R). For a PSF having a radius of five pels, a total of eighty points reside on a total of only thirteen concentric rings. However, since the number of rings (therefore the number of multiplications) can grow very large, an approximation is used to simplify the situation further: One assumes that, near the outer edges of the PSF, the values of h(R) on several closely spaced rings can all be approximated by some average value $h(R')$. This effectively groups several adjacent rings into one annulus to which the single filter coefficient $h(R')$ is assigned.

The particular approximation used in this research involved defining annuli one pel wide for all values of radius greater than five pels. Various experiments used PSF's as large as nineteen pels in radius. Although the "annulus approximation" distorts the shape of a point spread function larger than five pels in radius, no experiments ever demonstrated filtering artifacts traceable to this shape distortion. It is conjectured that this shape distortion will not, in most cases, produce visible artifacts in filtered images. Whether the "annulus approximation" can be extended to radii smaller than five pels without producing visible artifacts is an appropriate subject for future experiments.

The statements above lead to a new expression of the convolution sum:

$$B(n_1,n_2) = \sum_{j=0}^{N_A} c_j \cdot \sum_{i=1}^{P_j} b_{ij}^{n_1,n_2}$$

Henceforth, each individual ring or annular group of rings will be referred to as an "annulus". Using that nomenclature, the inner summation in the equation above is the "annulus sum" of all values of the input b on the jth annulus around the point (n_1,n_2). (There are P_j points on that annulus.) The product of the "annulus sum" and the "annulus coefficient" (or "filter coefficient") c_j is the "annulus product". The grand total of the annulus products for all $N_A + 1$ annuli is the convolution sum for the single output value $B(n_1,n_2)$. (The "annulus" corresponding to j=0 has zero radius and is not a true annulus. c_0 is simply the value of the PSF at its central point.) A few of the properties of this new formulation are immediately evident. First, storing several filters in the filtering program is very simple since the number of annulus coefficients is of the order of R, the radius of the PSF in pels. If several filter functions are available, a different one can be selected for each pair of indices (n_1,n_2) before evaluation of the annulus sums begins. $N_A + 1$ multiplications are required for each value of the output function $B(n_1,n_2)$. Consistent with the "annulus approximation" discussed above, N_A equals R + 8 when $R \geq 5$ pels. N_A is not only of the order of R, but is also linearly dependent on R. For

small values of R, the number of multiplications is equal to or less than the number of multiplications used by FFT procedures [17,18,19]. However, the number of additions is of the order of R^2 and is functionally dependent on R^2. This is a distinct disadvantage compared to FFT processes.

An important implementation problem of this algorithm is identifying the pels residing on a given annulus around a given central pel. The problem is complicated by the one-dimensional rather than two-dimensional addresses of memory locations in which the eight-bit pels are stored. However, one can define a central pel with a known memory address as the (0,0) origin of some Cartesian coordinate system. Then another pel residing on some distant annulus has the integer coordinates (m,n). Several lines of the input picture reside in memory at one time. Each line has a fixed length of L pels, which includes the extra pels on the left and right borders of the line. No matter what the memory address of the (0,0) pel, the address offset of the (m,n) pel relative to the (0,0) pel is given by:

$$n \cdot L + m$$

All that is required to identify the pels on a particular annulus is the memory address of the current central pel and a list of fixed address offsets for the surrounding pels in the "upper half plane" (where values of n are positive). This is because the offset for the "lower half plane" pel (-m,-n) is the negative of the offset for (m,n).

During its initialization phase, the filtering program creates a list of address offsets for each annulus defined for the filter function in current use. These lists are made from lists of integer coordinate pairs (m,n) representing points in Cartesian space within a 19-unit radius of the point (0,0). The coordinate pairs are also grouped according to the annuli to which they are defined to belong. To conserve memory space, only the coordinate pairs for points in the angular slice between zero and 45 degrees are stored as basic data. The four-fold and eight-fold symmetries mentioned above are used to generate other coordinate pairs on the same annulus.

As explained above, input picture lines are read in one at a time, after the first several lines have been read in at once. If computer memory is thought of as two-dimensional, then the picture line to be filtered is the one in the "middle" of the multiple line array. The convolution process uses the lines "above" and "below" it. If the processing of lines proceeds from the top to the bottom of the input picture, then the top line of the multiple line storage array is the one discarded when the filtering of the middle line is complete. The remainder of the array is moved upward one line, and space becomes available for a new input line at the bottom of the array. The movement is done by moving the pels to new memory locations, rather than by changing pointers to picture lines. The process is similar to the high-speed "recompacting" done on program address spaces by operating systems which utilize relocatable partitioning. In this

way, the input picture lines are filtered sequentially in one pass, and the ordering of the pels relative to each other in computer memory remains consistent. This allows the address offsets computed at the beginning of the process to remain fixed throughout. A pointer to the pels on the middle picture line defines the memory addresses of the centers around which the annulus sums are evaluated. This pointer is reset to the same address each time a new middle line is begun. It is incremented by one, from one pel to the next on that line.

Another basic implementation issue was decided by the characteristics of PDP 11/40 fixed-and floating-point hardware. The convolution sum calculations were programmed in fixed-point arithmetic as:

$$\underline{B}(n_1,n_2) = \sum_{j=0}^{N_A} I_j \cdot \sum_{i=1}^{P_j} b_{ij}^{n_1,n_2}$$

All values of the input image b are treated as eight-bit integers in the range [0,255]. The annulus sum is evaluated using one 16-bit register. Each filter coefficient c_j is multiplied by some scale factor 2^S and rounded off to a signed 15-bit integer I_j. S is chosen such that the c_j with the largest magnitude has an absolute value between 2^{14} and $2^{15}-1$. The annulus sum is multiplied by I_j and the entire 32-bit result is saved as the annulus product. This quantity is added to the convolution sum for $\underline{B}(n_1,n_2)$ in a 32-bit accumulator. When the summation is complete, two steps are necessary to convert a

32-bit value of $\underline{B}$ to an 8-bit value of B. The first step is division by 2^S (a right shift). The second step involves forcing the value of B, if necessary, into the range [0,255]. At each stage of the computation, overflow tests occur and appropriate actions are taken when overflows are detected. Appendix B shows a set of constraints which can be imposed on the annulus coefficients so that overflows do not occur and so that no value of B equals or exceeds 256.

The digital PSF's used for both nonadaptive and adaptive filtering were sampled Gaussian functions with radii of 5, 7, 10, 13, 15, and 19 pels respectively. If the Gaussian "spread" parameter σ is measured with the distance between pels as the unit distance, then the radii named above equal 4.47 times their respective σ values. $4.47 \cdot \sigma$ was used because the Gaussian annulus coefficients vary over several orders of magnitude. The use of 15-bit signed integer coefficients in the filtering computations required truncation of the Gaussian functions to a radius approximately equal to $4.47 \cdot \sigma$. Figures 3A and 3B show two-dimensional radial cross-sections of a continuous unit-volume Gaussian PSF h(r) and its Fourier-Hankel transform H(q). The unit of measure for r and σ is one arbitrary pel distance. The sampled version of h(r) therefore has an effective radius of ten pels. The annulus coefficients for this digital PSF appear in Table I. Since the sample values are scaled so that the sequence has unit energy, the annulus coefficients vary somewhat from the corresponding values of h(r). This is due to the distortions caused first by sampling and

ANNULUS NUMBER	RADIUS	COEFFICIENT
0	r = 0	.032031
1	1	.028933
2	$\sqrt{2}$	.026180
3	2	.021435
4	$\sqrt{5}$	.019394
5	$\sqrt{8}$	.014368
6	3	.013000
7	$\sqrt{10}$	.011763
8	$\sqrt{13}$	.008715
9	4	.006454
10	$\sqrt{17}$	.005842
11	$\sqrt{18}$	.005287
12	$\sqrt{20}$	.004328
13	5	.002625
14	$5<r\leq 6$	.001553
15	$6<r\leq 7$	.000467
16	$7<r\leq 8$	.000114
17	$8<r\leq 9$	.000023
18	$9<r\leq 10$	.000004

TABLE 1. ANNULUS COEFFICIENTS (c_j's) FOR DIGITAL GAUSSIAN PSF WITH RADIUS = 10 PELS

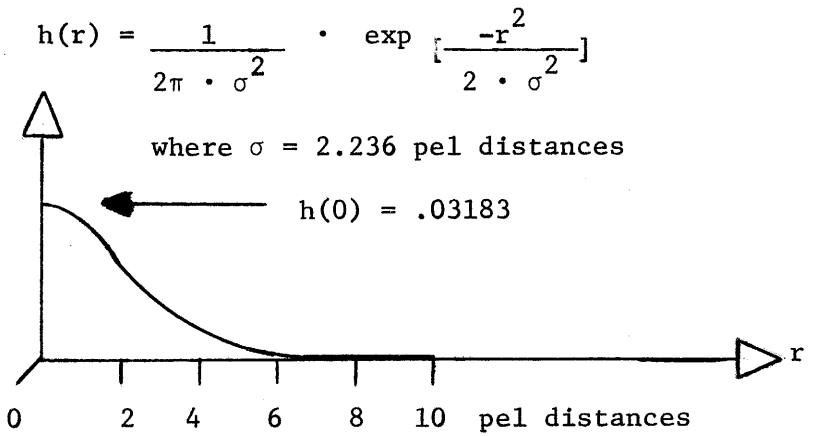

FIGURE 3A. CROSS-SECTION OF CONTINUOUS 2-DIMENSIONAL GAUSSIAN PSF

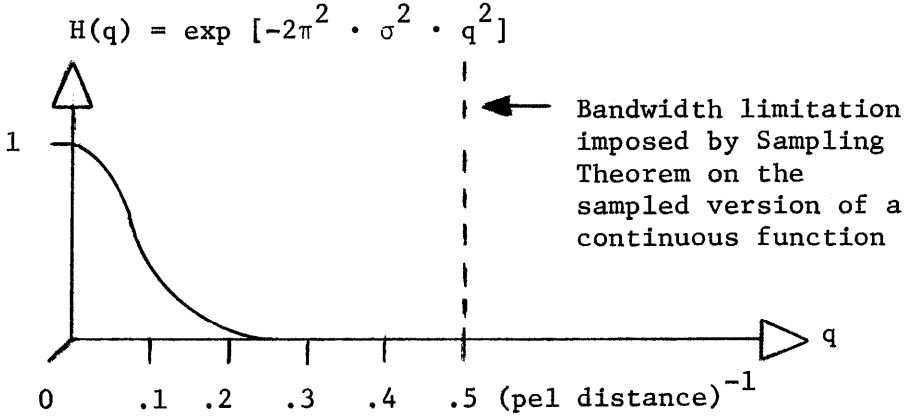

FIGURE 3B. CROSS-SECTION OF 2-DIMENSIONAL GAUSSIAN FREQUENCY RESPONSE

truncating h(r), then by applying the "annulus approximation" to the resulting sequence. The unit of measure for the radial frequency variable q is the reciprocal of the pel distance. When a continuous two-dimensional function is sampled on a Cartesian grid with a certain pel distance between samples, the Sampling Theorem imposes an upper limit on the bandwidth of the sampled function. In the units of measure of q, this limit is .5. It is evident from Figure 3B that a Gaussian impulse response ten "pel distances" in radius has a bandwidth (at -3db) of .0593. This is approximately one tenth of the bandwidth of any sampled image on which the sampled impulse response might operate.

A useful direction for further study might be the investigation of low-pass filters other than the Gaussian. Techniques have been published [20] for the design of two-dimensional digital filters with finite impulse response. There are also techniques [21] for "windowing" two-dimensional infinite impulse responses. "Windowing" is another device which permits one to sidestep the stability problems associated with two-dimensional recursive filters.

A discussion of the performance of the convolution algorithm is now in order. It should be noted, first of all, that the particular PDP 11/40 used for this research contained enough memory to accomodate even the 39 input picture lines required by the PSF with the 19-pel radius. As explained above, the input lines varied from 450 to 670 pels in length. For those computers with less memory, the "overlap-

save" technique is available [18]. This technique involves generating sections of output lines from the corresponding sections of several input lines. More than one pass must be made through the input image. For example, the first pass might read the left half of each input line and create the left half of each output line. The second pass would then process the right half of the image. Even though such a procedure was not needed for this research, experiments showed that the low-pass filtering was the computational "bottleneck" in the image enhancement software. Filtering generally took far more computation time than all other processes combined. These included the logarithmic and antilogarithmic transformations, the compression, the edge image generation, and even the selection of the different values of α used in adaptive filtering. Typical timings were as follows: When a 512 by 512 input image was filtered by a PSF ten pels in radius, approximately twenty output lines were generated per minute. When the PSF was 19 pels in radius, the rate was only six output lines per minute. This is undoubtedly due to the R^2 dependence of the number of additions. As will be shown in Chapter III, future implementations of the adaptive filtering techniques will not require convolutional filtering as was originally anticipated.

This concludes discussion of the filtering algorithm. Discussion of the other image enhancement software components follows.

C. IMAGE ENHANCEMENT SOFTWARE COMPONENTS:

LOGARITHMIC TRANSFORMATION AND TONE SCALE COMPRESSION

The logarithmic and antilogarithmic transformations are activated by software switches for nonlinear filtering experiments. Eight-bit values are converted between the brightness and log-brightness domains by high-speed table look-up. The logarithm table maps an integer b in the range [0,255] into another integer $\underline{b}$ in the range [0,255] using the rounded-off values of the function:

$$\underline{b} = 255 \cdot \frac{\ln(1 + .02 \cdot b)}{\ln(1 + .02 \cdot 255)}$$

The antilogarithm table is the inverse of the logarithm table. There were two reasons for using this transformation. First, it distorts the tone scale in a way similar to, but less severe than, the behavior of the $\log_{10}(Kb)$ function used in homomorphic filtering. Second, other experiments [22] have shown that its visual effects on images are in some sense optimal.

The dynamic range compression system compresses and rebiases the tone scale of the input brightnesses or log-brightnesses. (Note, in Figure 2, that the compression operates after the logarithmic transformation.) The transformation of the input brightness b to

the output brightness $\underline{b}$ is:

$$\underline{b} = f \cdot b + i$$

where f is the fraction less than one which causes the compression and i is an integer in the range $[0,(1-f) \cdot 255]$ which adds the bias. The various nonadaptive and adaptive filtering experiments showed that the output images with the best appearance were produced by compression functions using these values: $f = \frac{15}{16}$, $i = 3$ for Laserphoto pictures and $f = \frac{13}{16}$, $i = 23$ for Polaroid pictures. These differences are due to three facts. The Polaroid pictures are smaller than the Laserphoto pictures and therefore the details in the pictures are harder to see. The high spatial frequency response of the scanner hardware is poorer than that of the Laserphoto hardware. The amplitude (brightness) response of the scanner-Polaroid film system is more nonlinear than the response of the Laserphoto-dry silver paper system, in the dark as well as the bright ends of the tone scale. Therefore, in general, Polaroid pictures required more edge sharpening, and therefore more compression, than could be used in Laserphoto pictures. Also, a larger bias was needed for the Polaroids to eliminate the very dark tones in which visibility of details was sometimes poor.

All of the software components used for nonadaptive filtering have now been described. The aims and results of this phase of the research will now be explained.

D. NONADAPTIVE FILTERING EXPERIMENTS AND RESULTS

It was expected that sharpening entire images with a fixed value of α would show the effect of that α on image details throughout the tone scale. It was also expected that the effect of each value of α would become even more evident if each α were used with a variety of Gaussian filter functions. The results of such studies would provide a range of α values to be used later in adaptive filtering experiments where α would become a function of brightness and contrast. Both linear and nonlinear filtering experiments were done, to verify the strengths and weaknesses of the logarithmic filtering technique.

The conclusions drawn from this and other phases of the research are based on examination of Laserphoto and Polaroid pictures by this investigator and a small number of other observers. As such, the conclusions drawn in this thesis are not rigorously "proven" by extensive psychophysical experiments. However, these conclusions do have sufficient experimental foundation to indicate the potential of the adaptive filtering techniques described here and to provide a direction for further work.

The conclusions drawn from the experiments in nonadaptive filtering are the following:

The range of useful α values seemed to lie roughly between $\alpha = 1$ and $\alpha = 5$ for Polaroid pictures and between $\alpha = .25$ and $\alpha = 2$

for Laserphoto pictures. The reasons for the larger α values associated with Polaroids were explained above. The lower limits corresponded to the minimum values of α which produced any noticeable edge sharpening. The upper limits corresponded to the maximum values of α which did not produce unacceptable artifacts in sharpened images. The artifacts observed in "oversharpened" images included excessive high frequency noise and excessive white and black halos at high contrast edges.

As was expected from the known brightness response of the human eye, the degree of sharpening which was tolerable or desirable at a given edge tended generally to increase with increasing brightness. Figures 4, 5, 6, and 7 are Laserphoto pictures in which this effect may be observed. Figure 4 is the unprocessed image and Figures 5, 6, and 7 are logarithmically filtered, each using a different value of α. As the value of α increases, the high-brightness low-contrast details (such as the high-rise buildings against the sky) become sharper. However, as α increases, details in the dark areas begin to appear unnatural. Two effects cause this. First, as high-frequency noise is amplified, it first becomes visible to the eye in dark areas. Second, highly sharpened details are most obvious to the eye in dark areas, and seem to stand out artificially, compared to similarly sharpened details in bright areas. Another effect visible as α increases is the increase of the white and black bands at the high-contrast edge between the coat and its brighter surroundings. Although most experiments showed that α should be smallest in dark

FIGURE 4. UNPROCESSED IMAGE

FIGURE 5. LOGARITHMICALLY FILTERED, WITH TONE SCALE COMPRESSION

α = .25, PSF RADIUS = 10

FIGURE 6. LOGARITHMICALLY FILTERED, WITH TONE SCALE COMPRESSION
α = .667, PSF RADIUS = 10

FIGURE 7. LOGARITHMICALLY FILTERED, WITH TONE SCALE COMPRESSION
α = 2, PSF RADIUS = 10

areas, some experiments indicated that α should sometimes be greater in the darkest tones than in the middle tones. This effect would enhance barely visible details in very dark areas if there are any such details. The nonlinear brightness response of films in very dark as well as very bright areas has already been mentioned. The problem of image details in very dark areas was the focus of some of the later experiments in adaptive filtering.

The radius of the Gaussian PSF proved to have a pronounced effect on the range of useful α values. The maximum useful value of α tended to decrease as the radius increased. One can account for this by noting that the larger the radius of the PSF, the wider the "tails" on peaks added to sharpened edges. Such a "tail" appeared artificial when amplified by too large a value of α. However, even the largest PSF's used (with radii of 15 and 19 pels) succeeded only in modifying the edges of most objects. The functions were not large enough to change the brightness of large areas.

Comparison of linear with logarithmic filtering verified the performance expected of the latter. "Asymmetric peaking" of edges definitely reduced the black bands produced at high-contrast edges by linear filtering. White halos on the bright sides of such edges were still visible. As expected, there was little or no visible difference between linear and logarithmic filtering where the enhancement of low-contrast details was concerned. Improved performance in this area had to be sought from some other nonlinear operator. Chapter III explains efforts to find such an operator.

EXPERIMENTATION WITH ADAPTIVE FILTERING

A. ADAPTATION TO LOCAL AVERAGE BRIGHTNESS

Chapter I has explained that a linear high-pass filter creates peaks at an edge whose amplitudes are proportional to the height of the edge and independent of the average brightness in the vicinity of the edge. However, the experiments mentioned above, along with extensive published evidence, indicate that the amplitudes of peaks should be related to the average brightness near an edge. This was the rationale used for attempting to add, at each pel in an image, the maximum acceptable edge sharpening consistent with the average local brightness. All adaptive filtering experiments aimed at this goal and two others. First, there should be no visible spurious boundaries between areas of an image with different degrees of sharpening. Second, abrupt large changes of brightness should receive minimal, rather than maximal, sharpening, since high contrast is inherently easy to see. Such sophisticated variations in the degree of sharpening were expected to permit more sharpening in bright areas than was possible with nonadaptive filtering. This proved to be the case, in the experiments.

Figure 8 is a diagram of the unsharp masking software used for the early adaptive experiments. In that software system, α is a function of the average image brightness in the vicinity of each pel,

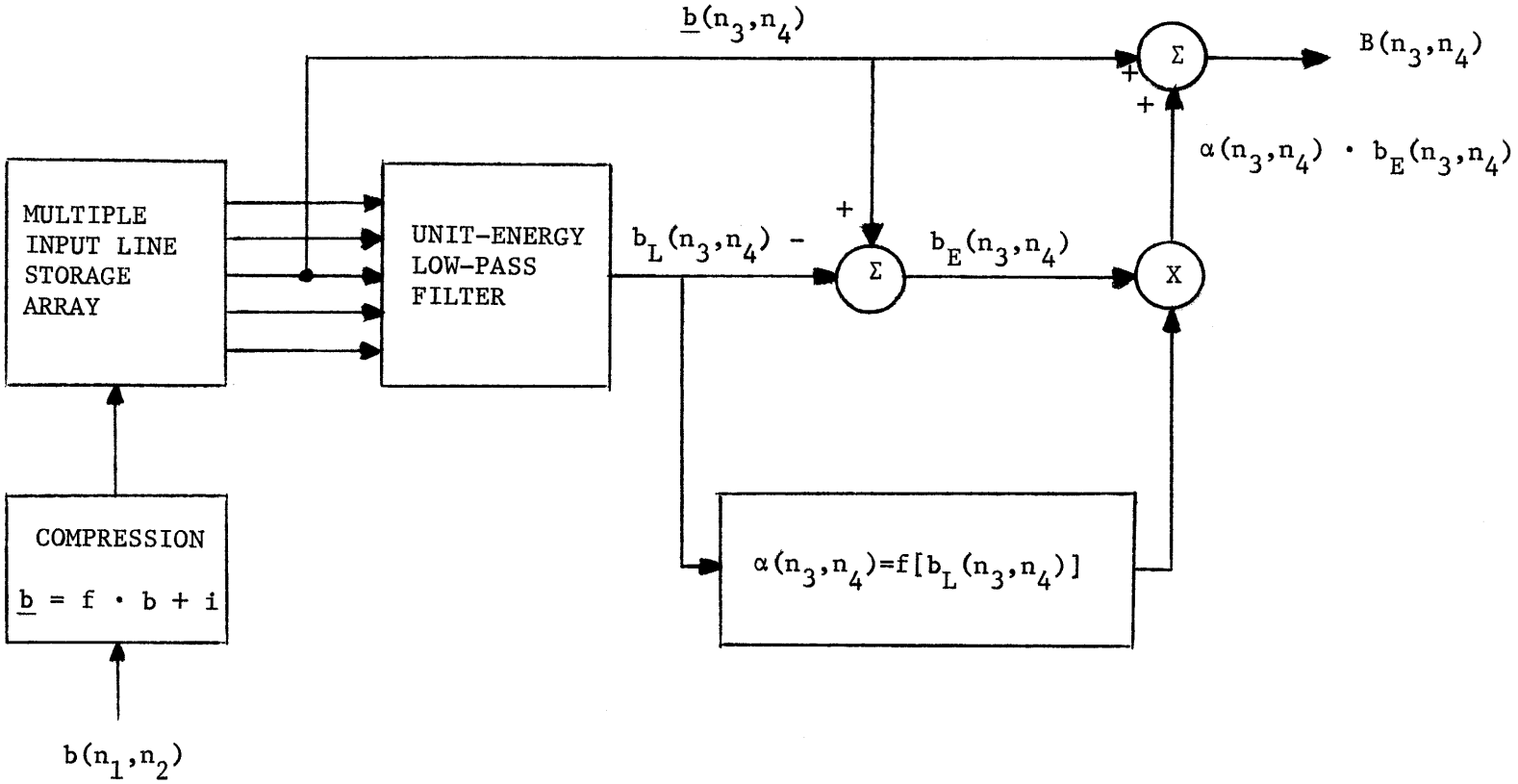

FIGURE 8. IMAGE ENHANCEMENT SOFTWARE SYSTEM FOR BRIGHTNESS - ADAPTIVE FILTERING

the average being taken to be the brightness of the low-pass filtered image. In terms of program implementation, the algorithm which selects α values scans the one available low-pass filtered picture line pel-by-pel. The brightness of each pel is compared with a set of three to eight thresholds which divide the tone scale into separate regions. A different value of α is assigned to each region. That value is used as a multiplier to scale the amplitude of the edge signal. The scaled edge signal is added to the brightness of the corresponding pel in the input image. This investigator surmised that modifying α from pel to pel would be faster and computationally simpler than changing low-pass filter functions. Experiments showed that the process of selecting α values was very fast, even when contrast was added as a selection criterion. The technique of modifying α alone was further justified by the satisfying results it produced.

Figures 9 and 10 are graphs of α as a function of the blurred image brightness b_L. These graphs show α to be constant over large ranges of tones. Therefore, in image areas of relatively constant average brightness, an adaptive filter using these functions behaves like the simple linear filter of Figure 2. Experiments showed no visible boundaries between image areas with different α values, whether the tone scale was coarsely divided (three thresholds) or finely divided (eight thresholds).

The graphs are typical of the α functions used in two types of experiments. The first type dealt with Laserphoto pictures, and α

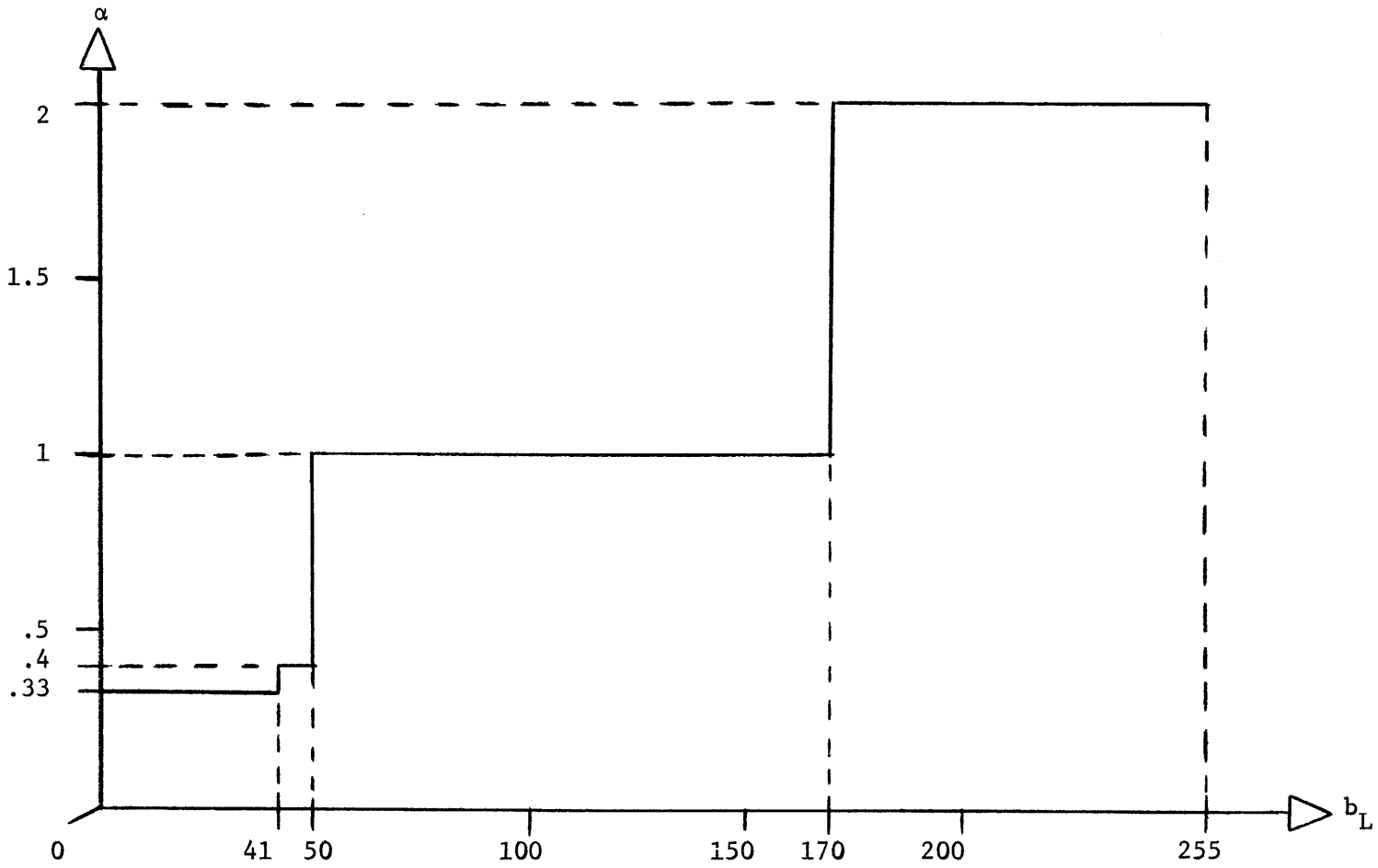

FIGURE 9. SHARPENING COEFFICIENT α AS A FUNCTION OF BLURRED IMAGE BRIGHTNESS b_L

THIS FUNCTION WAS USED TO PRODUCE LASERPHOTO PICTURES

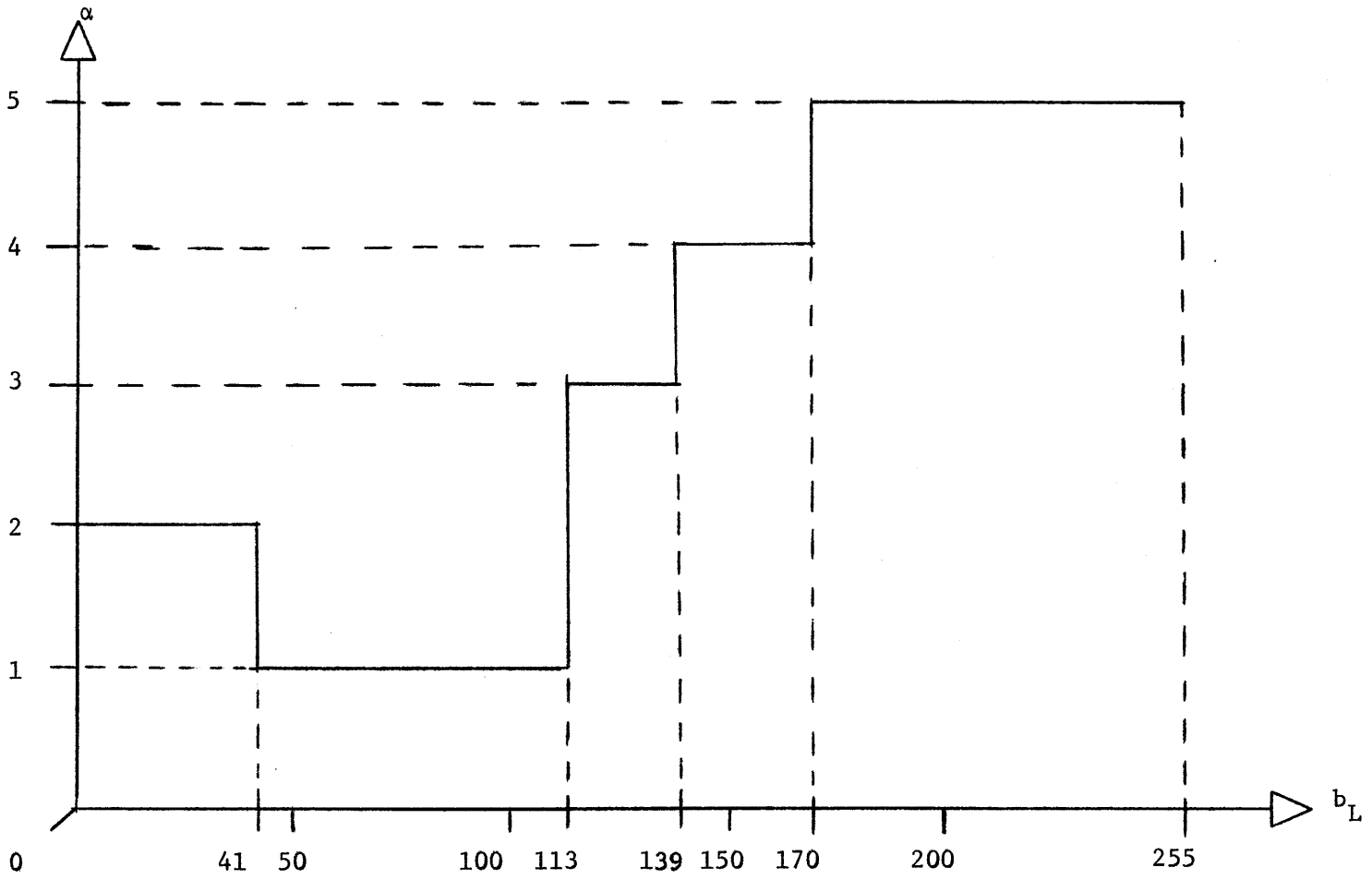

FIGURE 10. SHARPENING COEFFICIENT α AS A FUNCTION OF BLURRED IMAGE BRIGHTNESS b_L

THIS FUNCTION WAS USED TO PROCESS POLAROID PICTURES

increased with increasing brightness, as in Figure 9. Certain predictable results were observed. Low-contrast edges in bright areas appeared more nearly equal in sharpness to low-contrast edges in dark areas. The use of minimal sharpening in dark areas reduced the black saturation on the dark sides of high-contrast edges. However, since the bright sides of such edges were subject to maximal sharpening, white halos remained. The effect was unacceptably similar to the asymmetric peaking produced by logarithmic filtering.

The second type of experiment involved Polaroid pictures. Since the Polaroids suffered most from poor visibility of details in very dark areas, α was made larger in the darkest tones than in certain middle tones. (See Figure 10.) Visibility of low-contrast details in very dark areas did improve, but at the expense of increased noise visibility and increased black saturation near high-contrast edges. The CRT-Polaroid system is an example of many image processing systems with finite dynamic range which exhibit some sort of S-shaped characteristic of output versus input brightness. Response to very low input brightness is a threshold phenomenon, while response to very high input brightness is a saturation phenomenon. It has been tacitly assumed in this thesis that degradations due to saturation affect the visible quality of an image more than do degradations due to thresholding. This investigator acknowledges that there may be many images with a great deal of detail in very dark areas, and that some imaging systems will severely degrade these details. The experiments discussed

above did not settle the issue of how such details should be enhanced without creating bad visible side effects.

B. ADAPTATION TO LOCAL AVERAGE BRIGHTNESS AND CONTRAST

Experiments showed that the adaptive filtering system of Figure 8 failed to solve the problem of halos at high contrast edges. This investigator therefore sought a method of reducing the sharpening at high-contrast edges, while preserving the dependence of low-contrast edge sharpening on average brightness. The software system of Figure 11 is such a method. This system uses the amplitude of the edge signal $b_E(n_3,n_4)$ as a rough measure of the height of the nearest edge in the image. α increases linearly with the average brightness b_L. However, the slope of the line depends linearly on $|b_E|$, and in a negative way. Figure 12 shows a family of lines for α as a function of b_L, each line representing a different constant value of $|b_E|$. As that figure shows, the value of α at high brightness decreases with increasing $|b_E|$, until it becomes a constant for all $|b_E|$ greater than 32. In qualitative terms, this means that minimal sharpening is applied to all edges having an increment of brightness greater than some limit.

This dependence of α on b_L and b_E has a very interesting side effect. As is shown in Figure 11, the input image $\underline{b}(n_3,n_4)$ is sharpened, pel-by-pel, by adding to it:

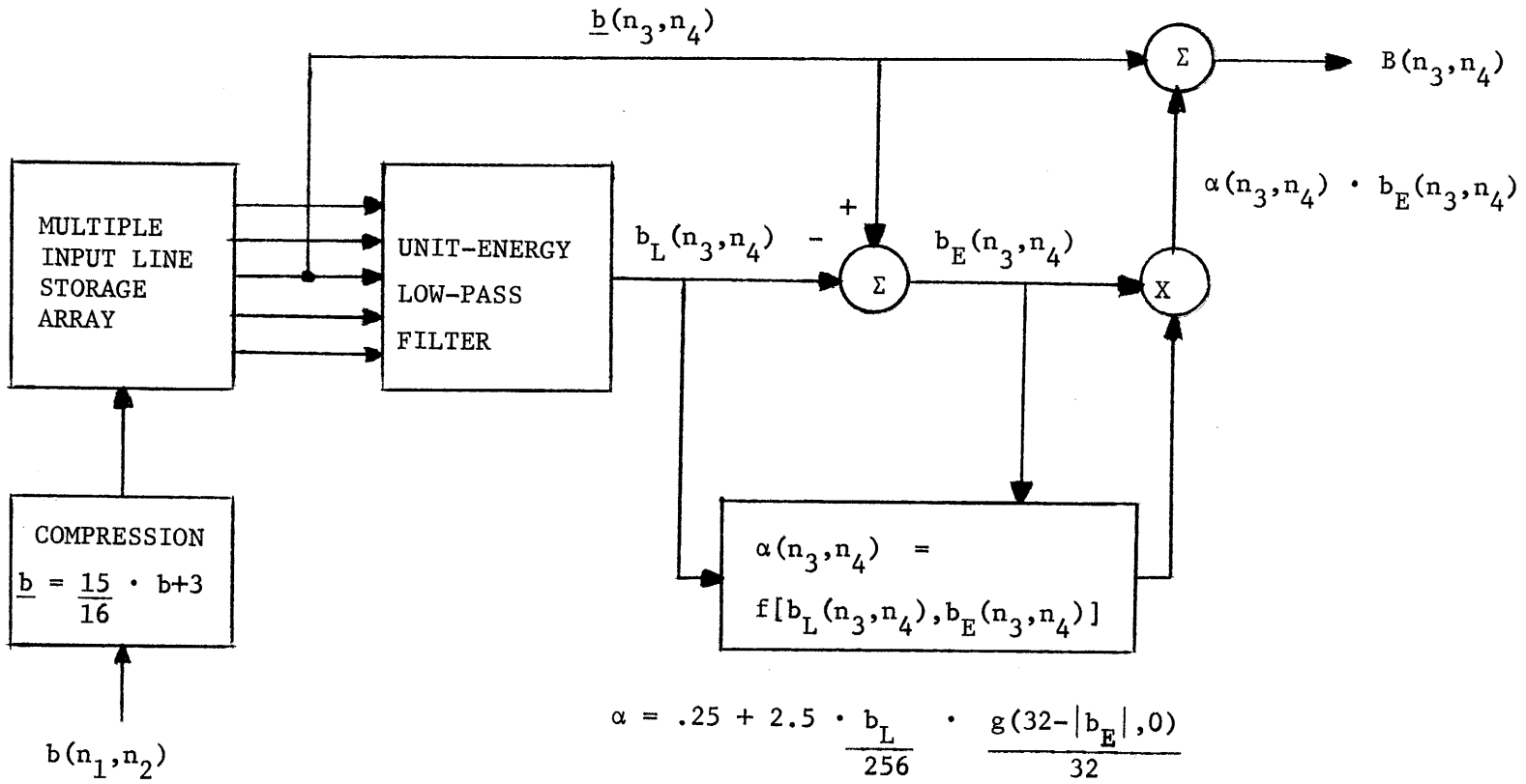

FIGURE 11. IMAGE ENHANCEMENT SOFTWARE SYSTEM FOR BRIGHTNESS - AND CONTRAST - ADAPTIVE FILTERING

$$\alpha = .25 + 2.5 \cdot \frac{b_L}{256} \cdot \frac{g(32 - |b_E|, 0)}{32}$$ where g(a,b) is the greater of a and b.

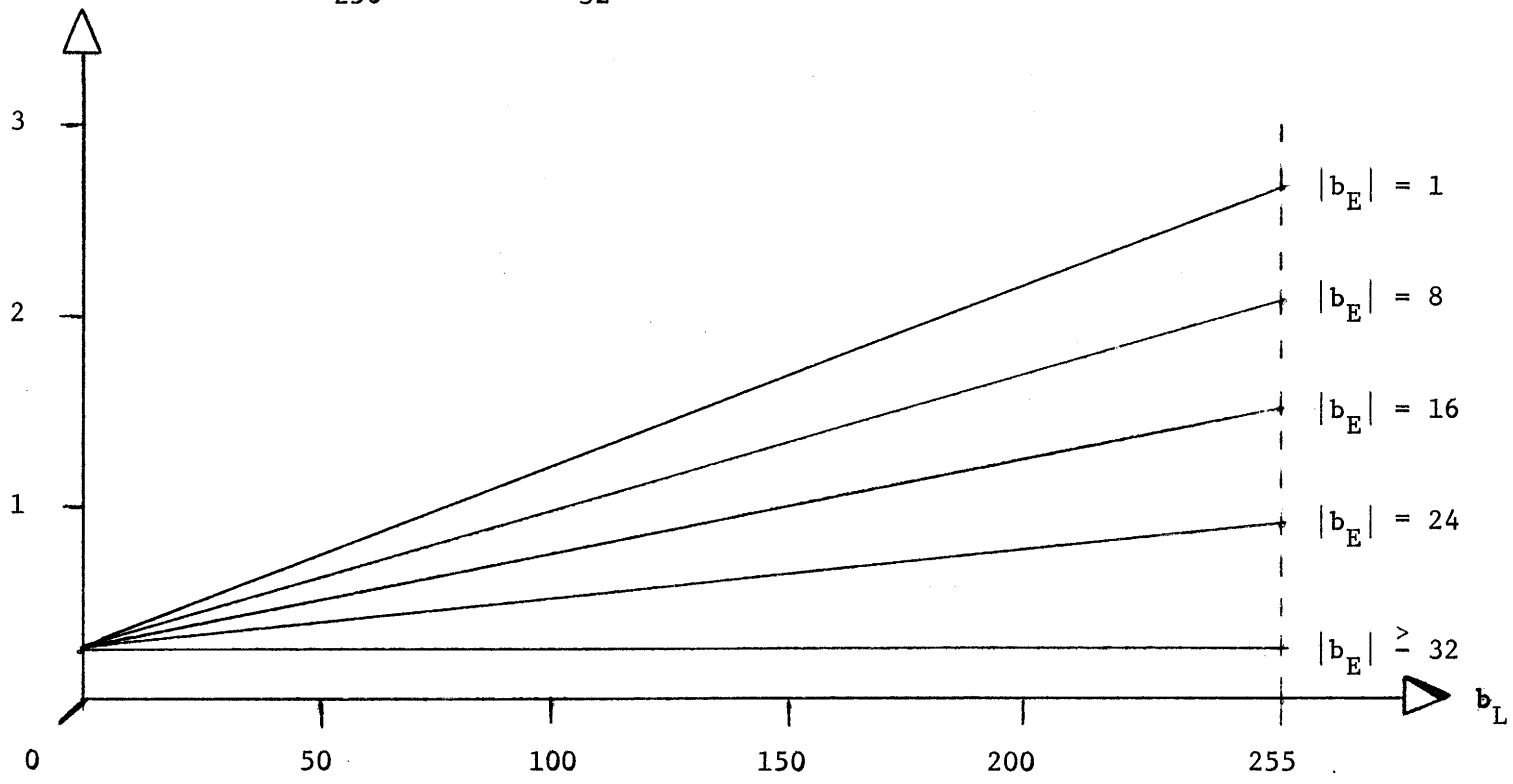

FIGURE 12. α FUNCTION USED FOR BRIGHTNESS - AND CONTRAST - ADAPTIVE FILTERING

$$\alpha \cdot b_E = [.25 + 2.5 \cdot \frac{b_L}{256} \cdot \frac{(32 - |b_E|)}{32}] \cdot b_E$$

$$= .25 \cdot b_E + 2.5 \cdot \frac{(\underline{b} - b_E)}{256} \cdot \frac{(32 - |b_E|)}{32} \cdot b_E$$

(This assumes that $|b_E| \leq 32$.) Since only one term in the above expression is linear in b_E, it is evident that multiplication of the edge signal by α not only scales that signal's magnitude, but also changes its shape. Figure 13 is a graph of the change of shape of a typical high-contrast edge signal. Figure 14 is a picture of the edge image $b_E(n_3,n_4)$ associated with the cameraman photograph of Figure 4. (A brightness bias of 32 has been added.)

This adaptive technique had a profound effect on high-contrast edges in Laserphoto pictures. Figure 15 shows the adaptively filtered version of the cameraman photograph. The α function graphed in Figure 12 was used to process this and other Laserphoto pictures. Note that the degree of sharpening in dark areas is only weakly dependent on contrast. The values of α at low brightness are nearly equal to the α value used for all high-contrast edges. This value of .25 was judged to be the minimum which produced visible sharpening. The value of α at high brightness and low contrast approaches 2.75. This value is significantly higher than the "maximum useful value" of 2 found in the nonadaptive experiments. The opinions of some

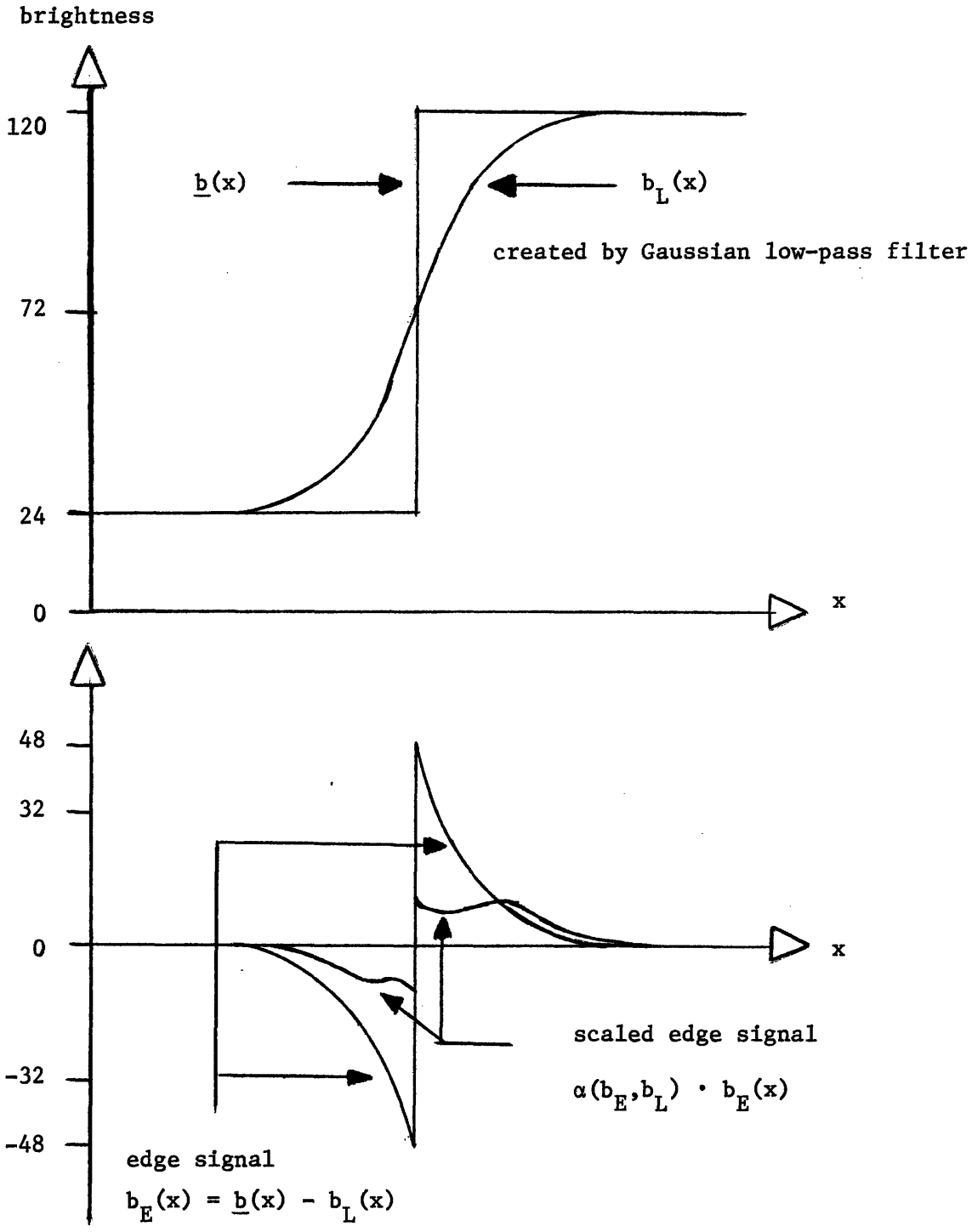

FIGURE 13. VARIATION OF A SCALED EDGE SIGNAL WHEN SCALE FACTOR α IS A FUNCTION OF EDGE SIGNAL AMPLITUDE

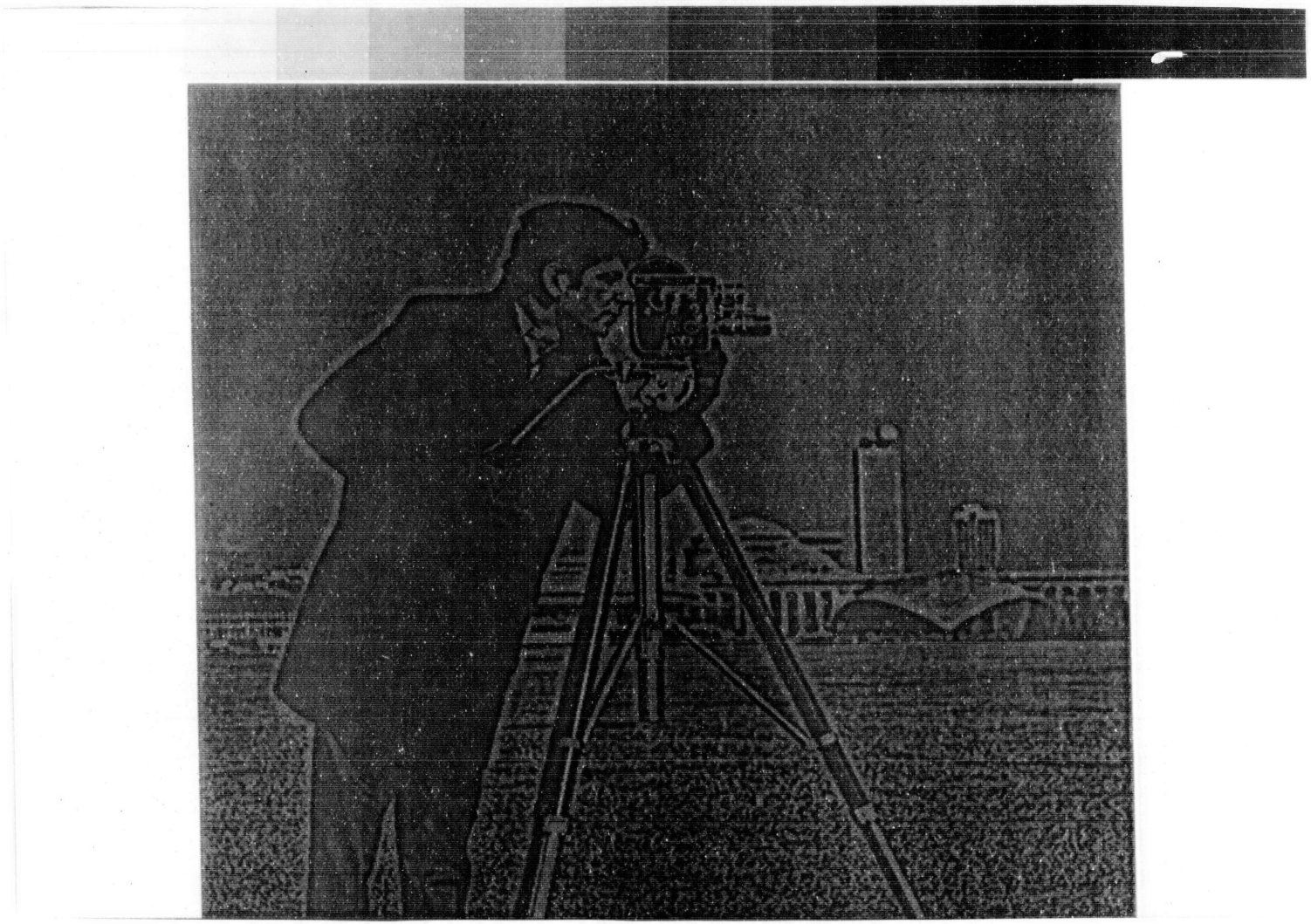

FIGURE 14. EDGE IMAGE DERIVED FROM FIGURE 4
BY ADAPTIVE FILTERING AND TONE SCALE COMPRESSION
BRIGHTNESS BIAS = 32, PSF RADIUS = 10

FIGURE 15. ADAPTIVELY FILTERED, WITH TONE SCALE COMPRESSION

PSF RADIUS = 10

observers indicated that, for some of the pictures processed in these experiments, that maximum α value might have been made still higher.

One can further compare the effects of adaptive and nonadaptive filtering in Figures 16 thru 30. Each group of three pictures contains an unprocessed image, an image logarithmically filtered using $\alpha=2$, and an adaptively filtered image. The image of Figures 16 thru 18 is a particularly interesting case. This is an aerial photograph of Lake Erie with Windsor, Ontario at the top and Cleveland, Ohio at the bottom. The photo is a radar echo image made by an aircraft equipped with side-looking all-weather radar. This photo, and others like it, are made regularly by NASA and the Air Force during each winter, to show the ice accumulations on all of the Great Lakes. NASA transmits these photos by facsimile to ships on the Great Lakes as a navigation aid. In Figures 16 thru 18, it is evident that the facsimile images benefit greatly from any kind of edge sharpening, and that adaptive edge sharpening produces fewer edge artifacts than the logarithmic technique.

These experiments in adaptive filtering were not extensive enough to permit conclusions about the "optimal" dependence of α on b_L and b_E. The function graphed in Figure 12 is simply that which produced the best Laserphoto pictures in these experiments. Full-scale psychophysical observer tests are the next logical step in the investigation of this technique. Two questions are pertinent in such tests. First, for what set of images and imaging systems can α functions be found

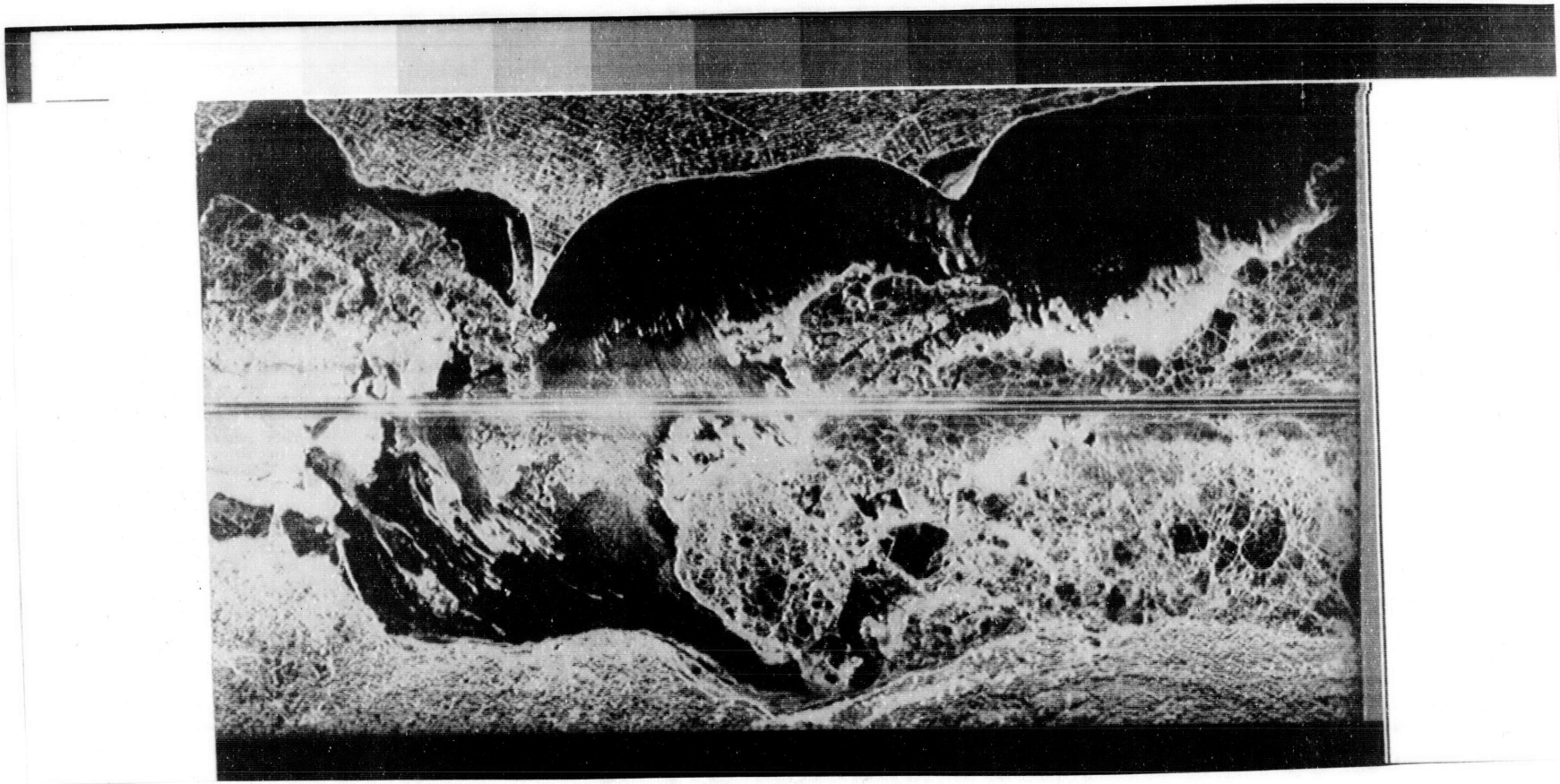

FIGURE 16. UNPROCESSED RADAR ECHO IMAGE

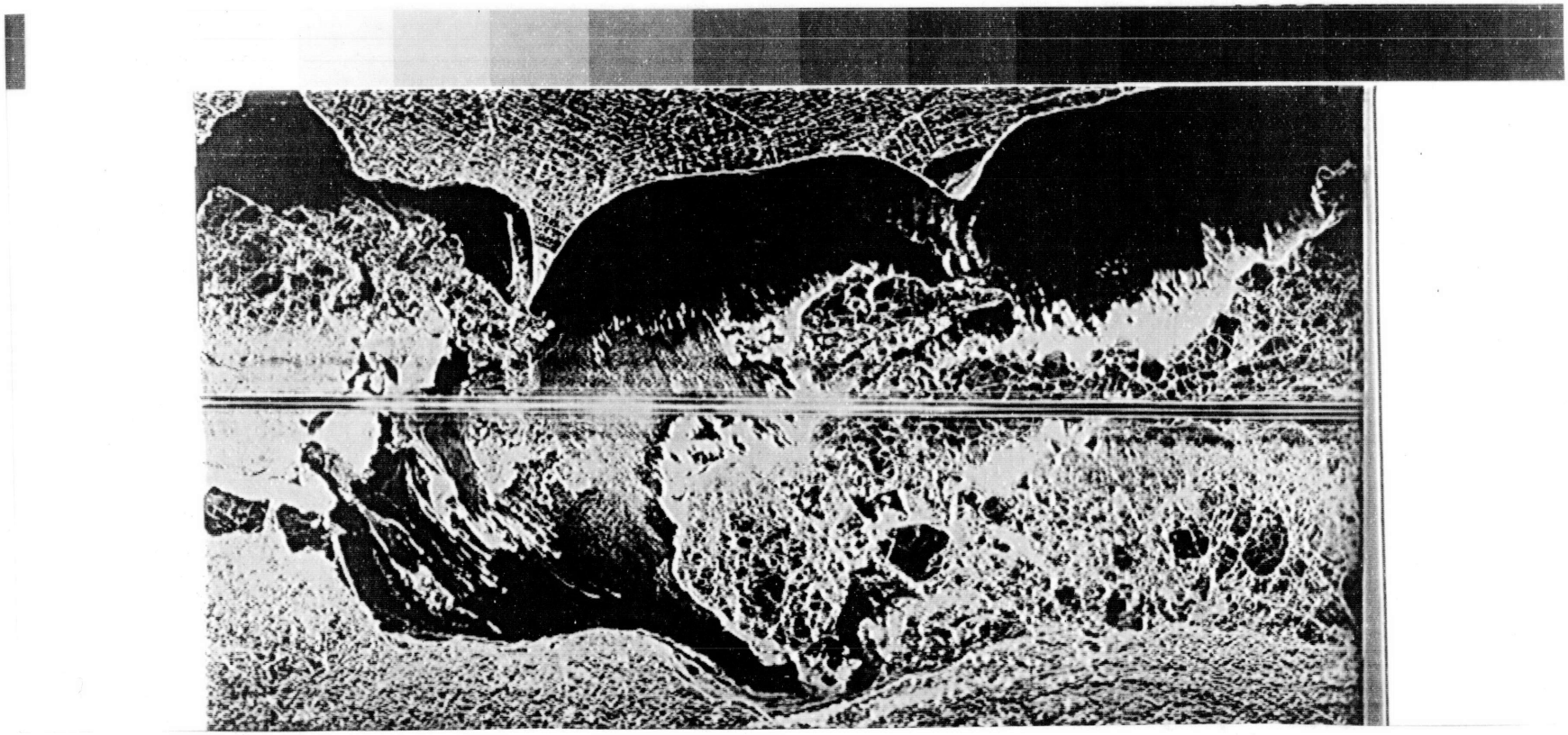

FIGURE 17. LOGARITHMICALLY FILTERED, WITH TONE SCALE COMPRESSION

α = 2, PSF RADIUS = 10

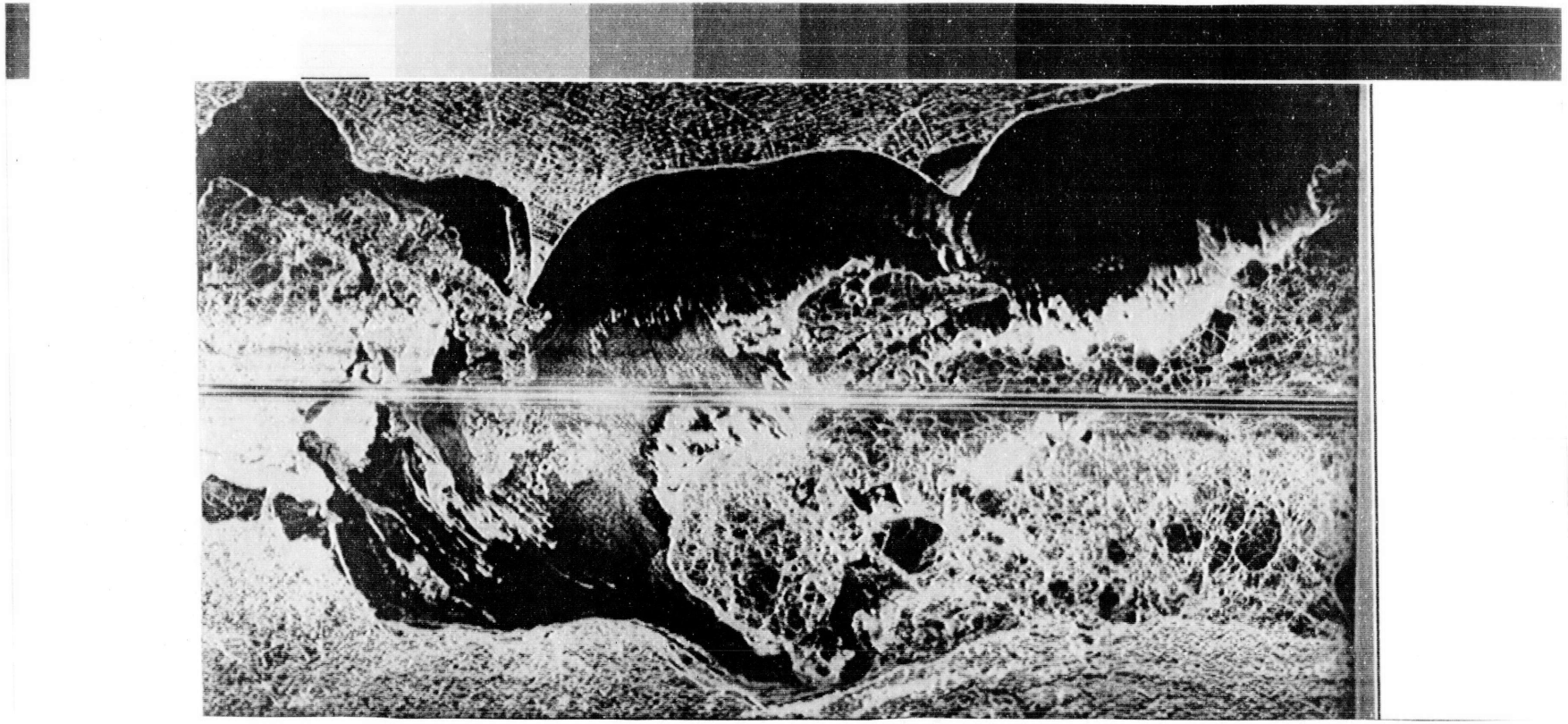

FIGURE 18. ADAPTIVELY FILTERED, WITH TONE SCALE COMPRESSION
PSF RADIUS = 10

which produce images superior to nonadaptively filtered images? Second, what are those optimal α functions?

Further testing of the adaptive algorithm can be made more efficient by one basic change to the low-pass filtering process. Since a single filter function produces the entire blurred image used in unsharp masking, the basic requirement for a convolution algorithm no longer exists. The Fast Fourier Transform can replace the convolution algorithm, and considerably reduce the computation time associated with large PSF's. There is available in the literature [23] an extensive discussion of how best to program the FFT to take advantage of computer memory and secondary mass storage. Another publication [24] explains a new and highly efficient algorithm for performing the matrix transposition which is a major intermediate step in two-dimensional FFT processing. Studies have been made [19,30] of the numbers of arithmetic operations involved in convolution and FFT processes. They show that filtering a typical 512 by 512 image is faster by FFT processing than by convolution, whenever the PSF has a radius greater than three or four pels. However, one should not conclude that useful adaptive filtering can be done only by FFT filtering with a large-diameter PSF. There are images such as aerial photographs and pictures of printed text, in which the details of interest are very small. (See Figures 16 thru 18 and 25 thru 27.) Experiments showed that visible improvements in the sharpness of such images can be made with point spread functions only five pels in radius.

FIGURE 19. UNPROCESSED IMAGE

FIGURE 20. LOGARITHMICALLY FILTERED, WITH TONE SCALE COMPRESSION
$\alpha = 2$, PSF RADIUS = 10

FIGURE 21. ADAPTIVELY FILTERED, WITH TONE SCALE COMPRESSION
PSF RADIUS = 10

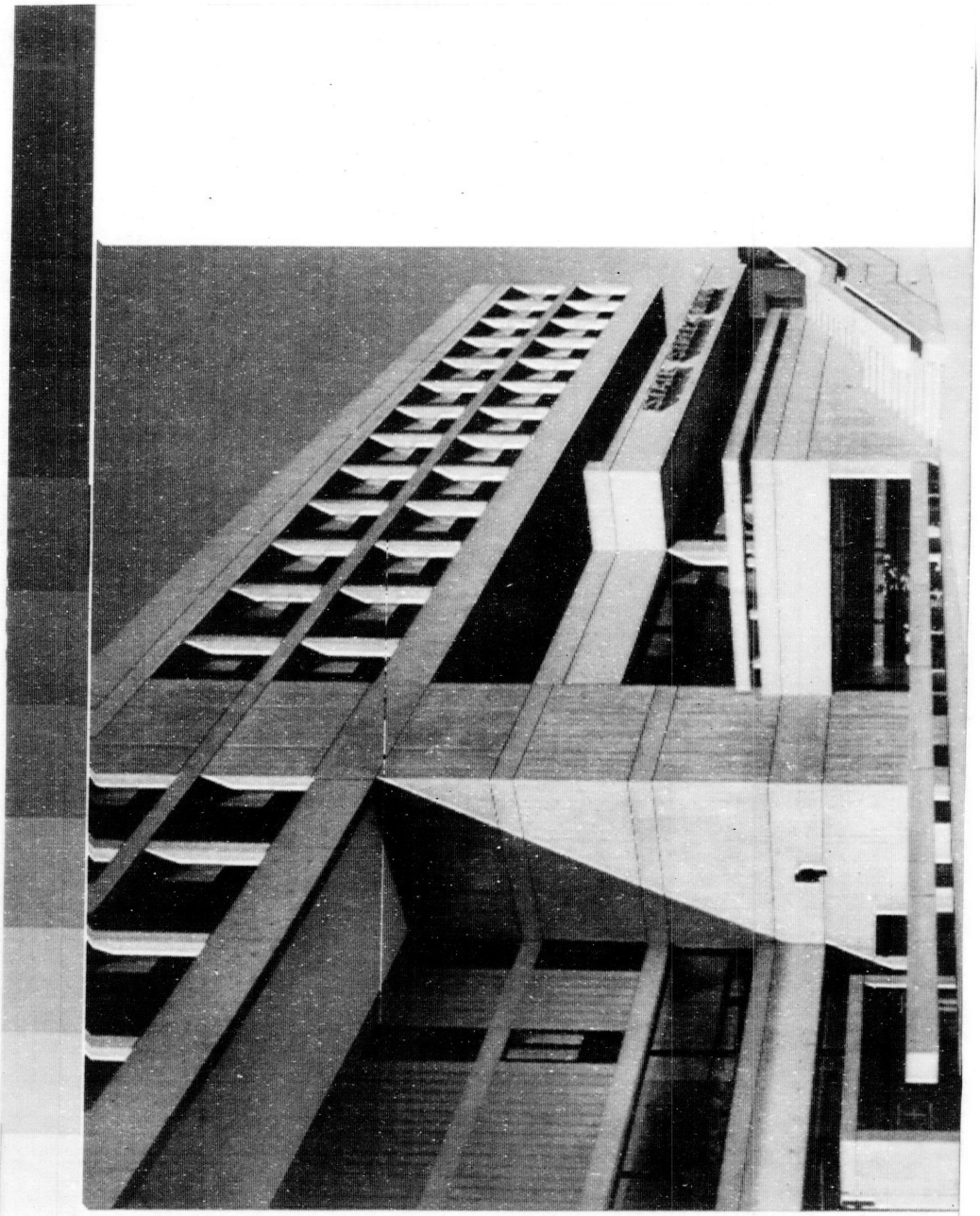

FIGURE 22. UNPROCESSED IMAGE

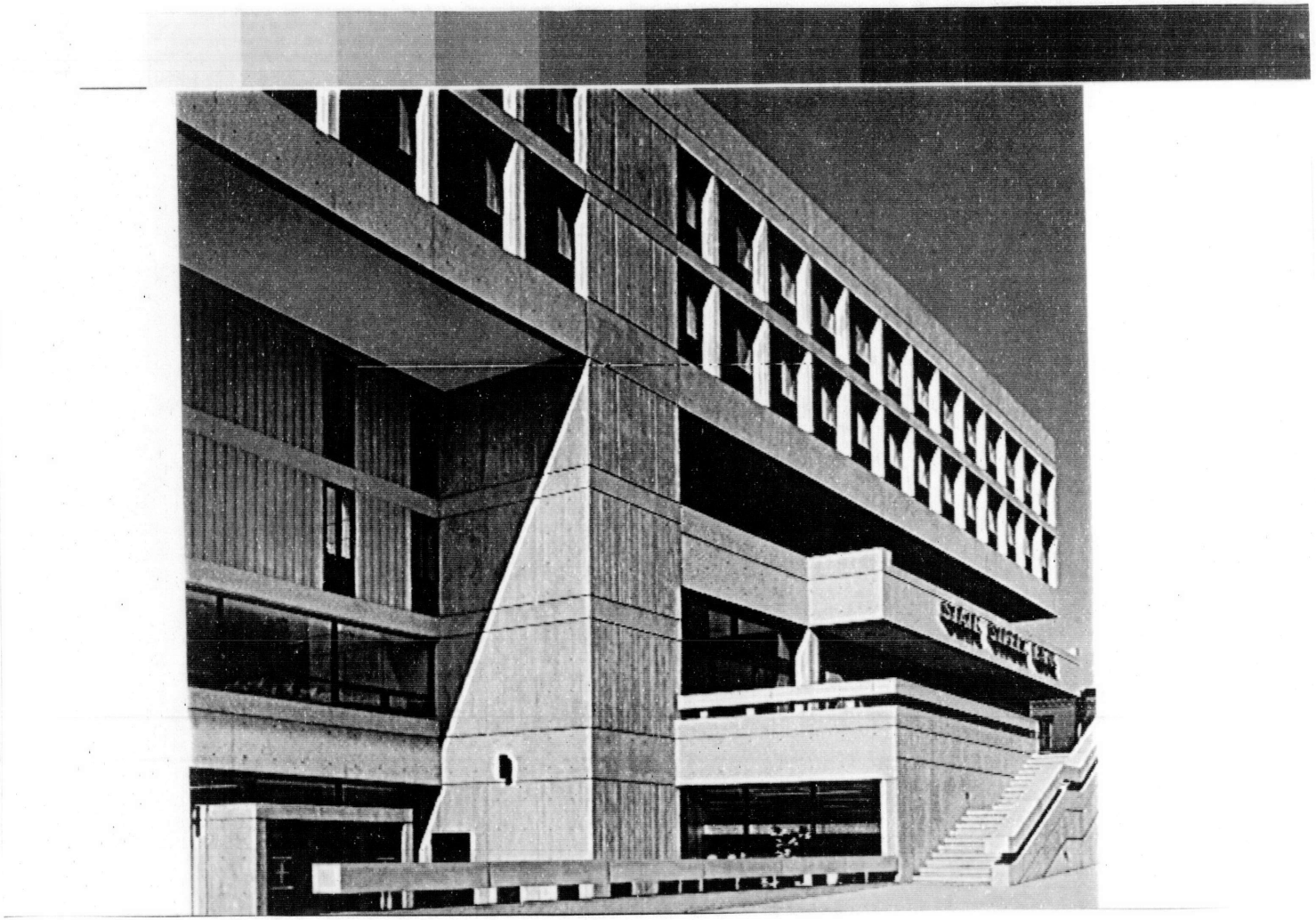

FIGURE 23. LOGARITHMICALLY FILTERED, WITH TONE SCALE COMPRESSION

α = 2, PSF RADIUS = 10

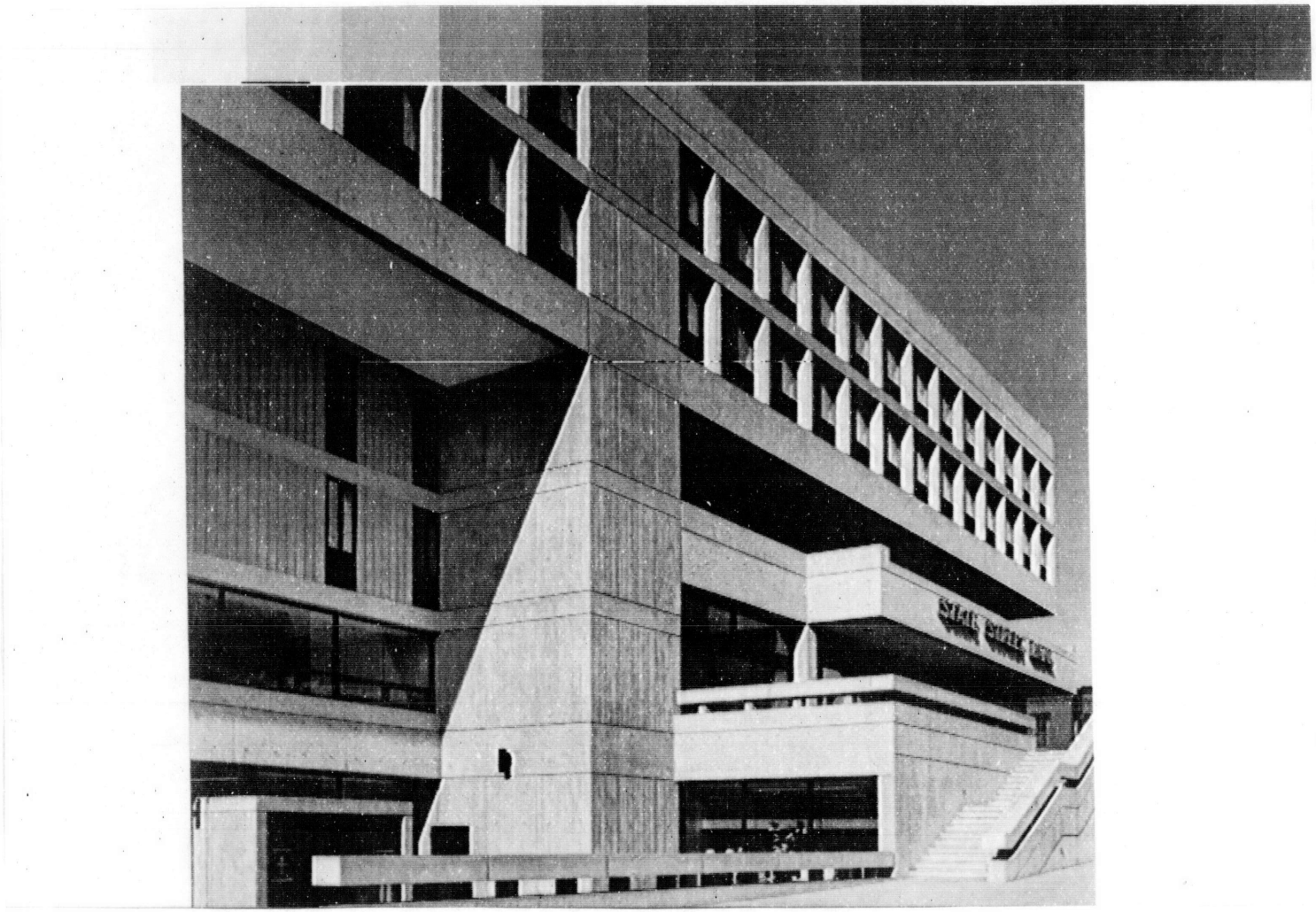

FIGURE 24. ADAPTIVELY FILTERED, WITH TONE SCALE COMPRESSION

PSF RADIUS = 10

FIGURE 25. UNPROCESSED IMAGE

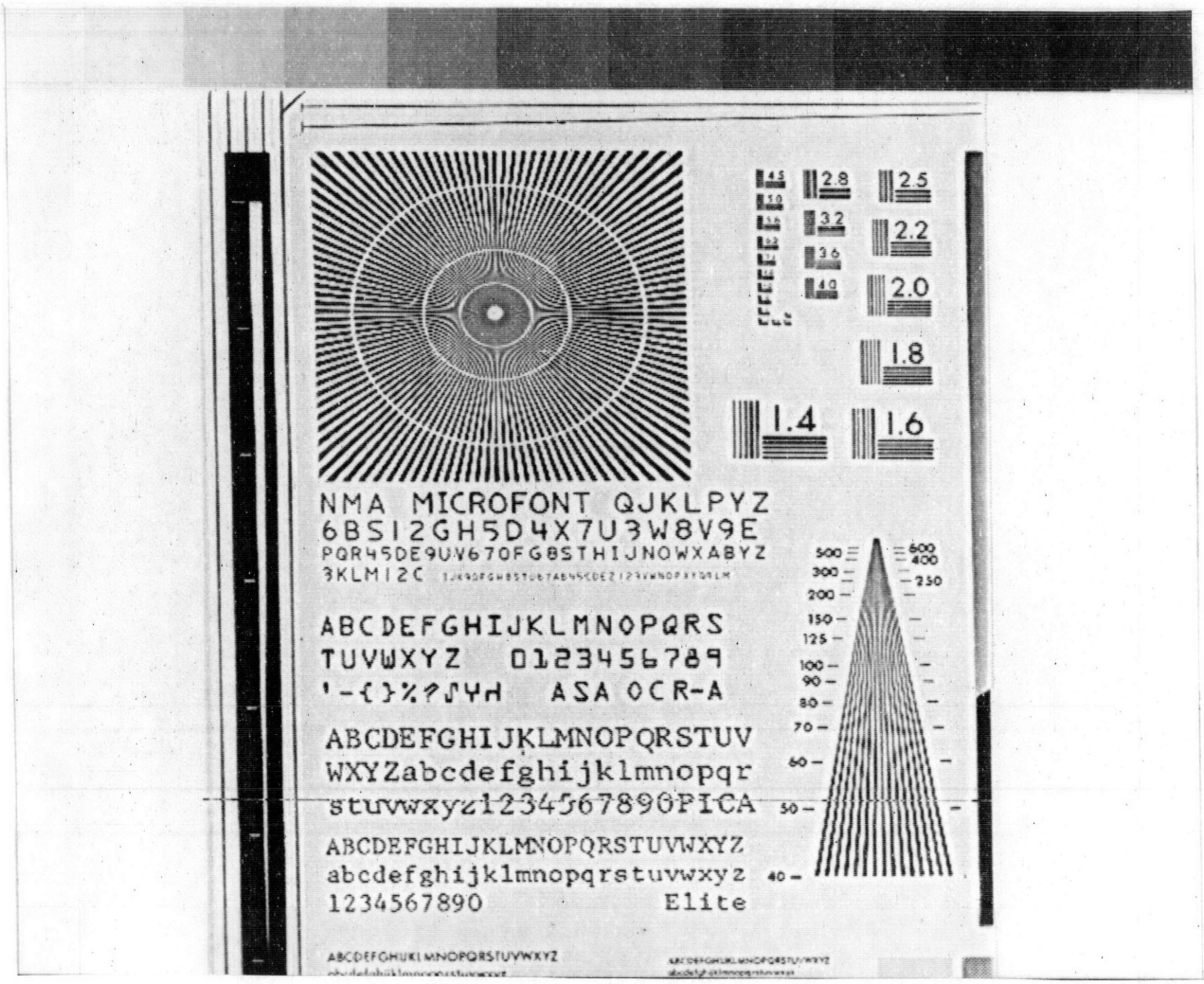

FIGURE 26. LOGARITHMICALLY FILTERED, WITH TONE SCALE COMPRESSION

α = 2, PSF RADIUS = 10

FIGURE 27. ADAPTIVELY FILTERED, WITH TONE SCALE COMPRESSION

PSF RADIUS = 10

FIGURE 28. UNPROCESSED IMAGE

FIGURE 29. LOGARITHMICALLY FILTERED, WITH TONE SCALE COMPRESSION
α = 2, PSF RADIUS = 10

FIGURE 30. ADAPTIVELY FILTERED, WITH TONE SCALE COMPRESSION
PSF RADIUS = 10

C. POTENTIAL APPLICATIONS OF ADAPTIVE UNSHARP MASKING

The power of the adaptive unsharp masking technique is the speed and simplicity with which it tailors the edge sharpening to the brightness and contrast at every single pel. This suggests a number of possible applications other than "after the fact" enhancement of already degraded images. Adaptive filtering might be used to preprocess images before they are transmitted by some irreversible (information lossy) coding system. The Roberts pseudorandom noise technique is such a system. It involves coarsely quantizing the brightness of an image to which pseudorandom noise has been added, to reduce the number of bits needed for transmission of the image. Even though the pseudorandom noise is removed from the received image, there remains in the image some noise caused by the original coarse quantization. Homomorphic filtering has already been used in some experiments [9] for pre- and post-transmission processing of Roberts-encoded images. The improvement in the quality of received images is quite evident. It is possible that adaptive unsharp masking might make even greater improvements. This is because positive values of α sharpen edges, while negative values of α act like a low-pass filter which might be used for "smoothing out" noise. These two effects suggest several possible combinations of adaptive pre- and post-processors, each aimed at solving some facet of the degradation problem. One idea for a single post-processor capable of simultaneously sharpening edges and removing noise is the following:

An α function may be devised which generates positive values of α only when the high-frequency edge signal amplitude, $|b_E|$, exceeds a certain threshold. When $|b_E|$ is below threshold, a negative value of α is generated. Note, however, that this scheme would require some knowledge of whether the noise in the image is additive or signal-dependent. It would also require a reasonably high signal-to-noise ratio in the images to be processed.

Other types of images can also benefit from adaptive edge sharpening and noise removal. It has been shown [25,26] that the image degradations caused by atmospheric turbulence can sometimes be characterized as the introduction of additive noise coupled with blurring by a zero-phase low-pass filter. Photographs degraded by atmospheric turbulence are therefore candidates for the same kind of processing as that suggested for Roberts-encoded images.

Quantum-limited images, such as medical radioisotope scans, present similar problems. Some adaptive filtering techniques have already been developed for such images [27,28]. These techniques take account of the observed fact that the noise in radioisotope scans is most pronounced in dark areas. The filtering technique is therefore to blur dark areas and to sharpen bright areas. To do this by adaptive unsharp masking, α would be assigned positive or negative values based on the average area brightness b_L, rather than on the edge signal b_E.

Images sent to earth from some satellites and spacecraft suffer from transmission at low power over a "noisy channel". Their high

spatial frequency response also suffers from technical compromises in the transmission hardware, which are forced by the need for bandwidth reduction. Many techniques [1,29] have been developed to restore the received image to the quality of the transmitted image. The implementation of adaptive unsharp masking in digital or analog hardware would be very straightforward. A satellite or spacecraft equipped with such hardware could sharpen an image adaptively before transmitting it to earth. The filtering operation could amplify high frequencies in the dark areas of the image where additive transmission noise is most visible. An adaptive filter on earth could then attenuate the high frequencies in the dark areas of the received image. This presumably would restore the normal appearance of the image while attenuating the transmission noise. Such applications as these would make adaptive unsharp masking a two-dimensional analog of the highly successful Dolby system used for acoustical noise reduction. This investigator has complete confidence that adaptive unsharp masking systems are capable of the same technical successes in the field of image processing.

APPENDIX A

THE EFFECT OF HIGH-PASS FILTERING ON A CHANGE IN BRIGHTNESS

Let brightness (b) be represented as a continuous function of position (x):

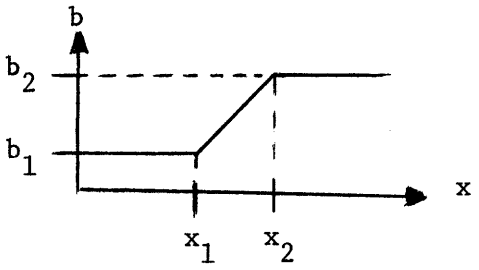

Let b(x) be filtered by the impulse response:

$$h(x) = (1+2\beta) \cdot \delta(x) - \beta \cdot k \cdot \exp[-k \cdot |x|]$$

where $k, \beta > 0$

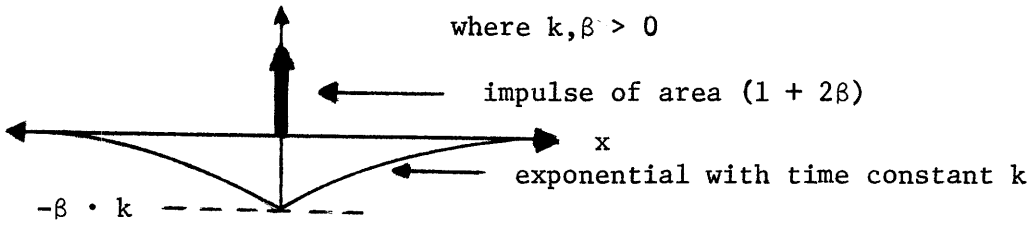

The frequency response associated with h(x) is:

$$H(f) = 1+2\beta - \frac{2\beta}{1 + \left(\frac{2\pi \cdot f}{k}\right)^2}$$

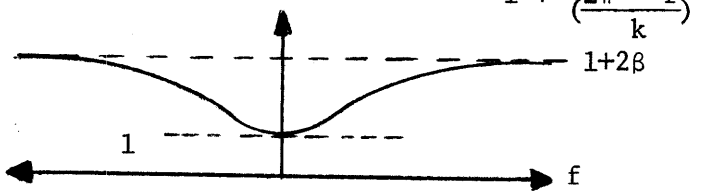

The result of convolving b(x) with h(x) is B(x):

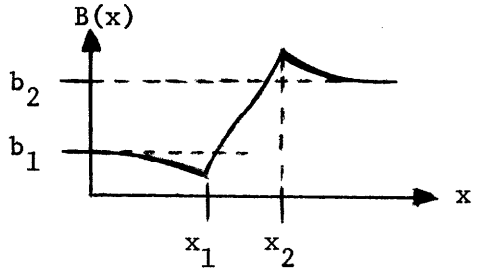

$$B(x_1) = b_1 - \frac{\beta \cdot (b_2-b_1)}{k \cdot (x_2-x_1)} \cdot (1 - \exp[k \cdot (x_1-x_2)])$$

$$B(x_2) = b_2 + \frac{\beta \cdot (b_2-b_1)}{k \cdot (x_2-x_1)} \cdot (1 - \exp[k \cdot (x_1-x_2)])$$

The effect of high-pass filtering is the "sharpening" of the edge between brightnesses b_1 and b_2. This is done by subtraction of an exponential edge signal on the dark side of the edge and addition of that edge signal on the bright side. The second term in each of the above equations expresses the maximum of the edge signal amplitude.

APPENDIX B

"NO OVERFLOW" CONSTRAINTS ON THE SET OF ANNULUS COEFFICIENTS $\{c_j\}$

Let the integer coefficient set $\{I_j\}$ be generated from the set $\{c_j\}$ via multiplication by 2^S and appropriate roundoff. Let input pels be eight-bits long:

$$0 \leq b_{ij}^{n_1,n_2} \leq 255$$

The convolution sum is evaluated as:

$$B(n_1,n_2) = \sum_{j=0}^{N_A} c_j \cdot \sum_{i=1}^{P_j} b_{ij}^{n_1,n_2}$$

This is implemented in fixed-point arithmetic by:

$$\underline{B}(n_1,n_2) = \sum_{j=0}^{N_A} I_j \cdot \sum_{i=1}^{P_j} b_{ij}^{n_1,n_2}$$

Constraint #1:

$$0 \leq B(n_1,n_2) \leq 255 \text{ iff } 0 \leq \sum_{j=0}^{N_A} c_j \cdot P_j \leq 1$$

If $\sum_{j=0}^{N_A} c_j \cdot P_j = 1$, then the digital PSF has unit energy and the average brightness and the dynamic range of the output image B are the same as those of the input image b. If

$\sum_{j=0}^{N_A} c_j \cdot P_j$ has some positive value other than 1, the average brightness of the image is either reduced or increased, and the dynamic range is either compressed or expanded.

Constraint #2: The annulus sum $\sum_{i=1}^{P_j} b_{ij}^{n_1,n_2}$ cannot overflow a 16-bit register as long as:

$$P_j \leq \frac{(2^{15} - 1)}{255} \simeq 128$$

(P_j is the number of points in the jth annulus around (n_1,n_2). For each PSF used in this thesis research, all values of P_j obey this constraint.

Constraint #3: The annulus product $I_j \cdot \sum_{i=1}^{P_j} b_{ij}^{n_1,n_2}$ cannot overflow a 32-bit register as long as:

$$-2^{31 - (S+8)} \leq c_j \cdot P_j < 2^{31 - (S+8)}$$

for each annulus coefficient c_j.

Constraint #4: The convolution sum $\sum_{j=0}^{N_A} I_j \cdot \sum_{i=1}^{P_j} b_{ij}^{n_1,n_2}$ cannot overflow a 32-bit register as long as:

$$-2^{31 - (S+8)} \leq \sum_{j=0}^{N_A} c_j \cdot P_j < 2^{31 - (S+8)}$$

Constraints 3 and 4 are obeyed by all of the unit-energy digital PSF's used in this thesis research.

BIBLIOGRAPHY

1. R. Nathan, "Picture Enhancement for the Moon, Mars, and Man", Pictorial Pattern Recognition, ed. by Cheng, Ledley, Pollock and Rosenfeld, Washington, D.C., Thompson, 1968, pp. 239-266.

2. M.M. Sondhi, "Image Restoration: The Removal of Spatially Invariant Degradations", Proc. IEEE, vol. 60, no. 7, pp. 842-853, July 1972.

3. T.S. Huang, W.F. Schreiber and O.J. Tretiak, "Image Processing", Proc. IEEE, vol. 59, no. 11, pp. 1586-1609, November 1971.

4. W.K. Pratt, "Generalized Wiener Filtering Computation Techniques", IEEE Trans. on Computers, vol. c-21, no. 7, pp. 636-641, July 1972.

5. W.F. Schreiber, "Wirephoto Quality Improvement by Unsharp Masking", Pattern Recognition Journal, vol. 2, pp. 117-121, September 1969.

6. S.W. Levine and H. Mate, "Selected Electronic Techniques for Image Enhancement", Proc. of the Society of Photo-optical Instrumentation Engineers, vol. 1, pp. 15-35, March 1963.

7. A.V. Oppenheim, R.W. Schafer, and T.G. Stockham, Jr., "Nonlinear Filtering of Multiplied and Convolved Signals", Proc. IEEE, vol. 56, no. 8, pp. 1264-1291, August 1968.

8. T.G. Stockham, Jr. "Image Processing in the Context of a Visual Model," op. cit. (2).

9. _____, "Intraframe Encoding for Monochrome Images by Nonlinear Filtering", Picture Bandwidth Compression, ed. by T.S. Huang and O.J. Tretiak, New York, Gordon and Breach, 1972, pp. 415-442.

10. S. Hecht, "Quantum Relations of Vision", Journal of the Optical Society of America, vol. 32.

11. F.W. Campbell, "The Human Eye as an Optical Filter", Proc. IEEE, vol. 56, no. 6, pp. 1009-1014, June 1968.

12. T.S. Huang, "Digital Computer Analysis of Linear Shift-Variant Systems", Evaluation of Motion-degraded Images, NASA publication SP-193, pp. 83-89, December 1968.

13. S.C. Som, "Analysis of the Effect of Linear Smear on Photographic Images", Journal of the Optical Society of America, vol. 61, pp. 859-864, July 1971.

14. C.W. Swonger and F.Y. Chao, "Computing Techniques for Correction of Blurred Objects in Photographs", op. cit. (12).

15. E.M. Granger, "Restoration of Images Degraded by Spatially Varying Smear", op. cit. (12).

16. A.P. Ginsburg, F.H. Cook and J.C. Mott-Smith, Image Analysis Facility: An Interactive Digital Computer System, Air Force Cambridge Research Laboratories Physical Sciences Research Paper no. 496, May 1972.

17. R.C. Borgioli, "Fast Fourier Transform Correlation Versus Direct Discrete Time Correlation", Proc. IEEE, vol. 56, no. 9, pp. 1602-1604, September 1968.

18. T.G. Stockham, Jr., "High-speed Convolution and Correlation", Spring Joint Computer Conference, AFIPS Proceedings, vol. 28, pp. 229-233, 1966.

19. E.L. Hall, "A Comparison of Computations for Spatial Frequency Filtering", op. cit. (2).

20. J.V. Hu and L.R. Rabiner, "Design Techniques for Two-Dimensional Digital Filters", IEEE Trans. on Audio and Electroacoustics, vol. AU-20, no. 4, pp. 249-257, October 1972.

21. T.S. Huang, "Two-Dimensional Windows", IEEE Trans. on Audio and Electroacoustics, pp. 88-90, March 1972.

22. B. Hashizume, "Companding in Image Processing", S.B. Thesis, Dept. of Electrical Engineering, Mass. Inst. of Tech., Cambridge, 1973.

23. B.R. Hunt, "Data Structures and Computational Organization in Digital Image Enhancement", op. cit. (2).

24. J.O. Eklundh, "A Fast Computer Method for Matrix Transposing", op. cit. (4).

25. J.L. Horner, "Optical Restoration Using Optimum Filter Theory of Images Blurred by Atmospheric Turbulence", op. cit. (12).

26. S. Morgan, Ed., Restoration of Atmospherically-degraded Images, NSF Summer Study Report, Woods Hole, Mass., 1966.

27. S.M. Pizer and H.G. Vetter, "Processing Quantum Limited Images", Picture Processing and Psychopictorics, ed. by Lipkin and Rosenfeld, New York, Academic Press, 1970, pp. 165-176.

28. D.A. Chesler, "Resolution Enhancement by Variable Filtering", Physics Research Laboratory, Mass. General Hospital, Boston, Internal Report, January 1969.

29. D.A. O'Handley and W.B. Green, "Recent Developments in Digital Image Processing at the Image Processing Laboratory at the Jet Propulsion Laboratory", op. cit. (2).

30. T.S. Huang, "Digital Fourier Analysis", Appendix 22, op. cit. (26).